CHALMERS

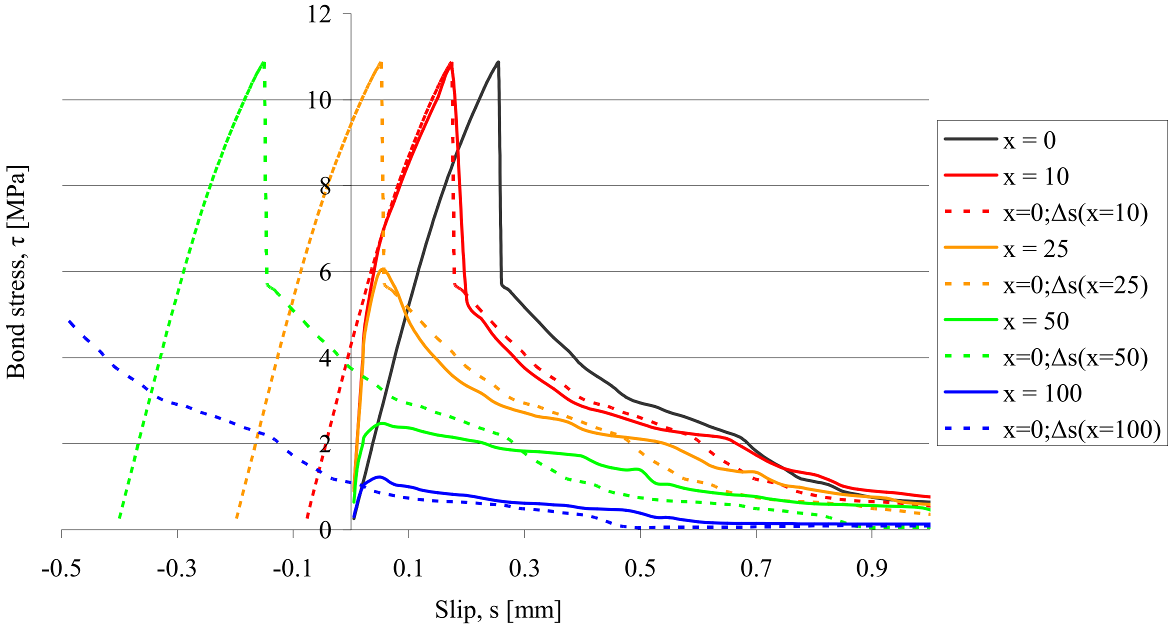

Bond of corroded reinforcement

Analytical description of the bond-slip response

Master's Thesis in the International Master's Programme Structural Engineering

HENDRIK SCHLUNE

Department of Civil and Environmental Engineering

Division of Structural Engineering

Concrete Structures

CHALMERS UNIVERSITY OF TECHNOLOGY

Göteborg, Sweden 2006

Master's Thesis 2006:107

MASTER'S THESIS 2006:107

Bond of corroded reinforcement

Analytical description of the bond-slip response

HENDRIK SCHLUNE

Department of Civil and Environmental Engineering
Division of Structural Engineering
Concrete Structures
CHALMERS UNIVERSITY OF TECHNOLOGY

Göteborg, Sweden 2006

Bond of corroded reinforcement
Analytical description of the bond-slip response
HENDRIK SCHLUNE

Master's Thesis 2006:107

Department of Civil and Environmental Engineering
Division of Structural Engineering
Concrete Structures
Chalmers University of Technology
SE-412 96 Göteborg
Sweden
Telephone: + 46 (0)31-772 1000

Cover:
Bond-slip curves for different corrosion penetrations, *x*, and shifted bond-slip curves for uncorroded reinforcement, for more information see Chapter 4.

Chalmers reproservice / Department of Civil and Environmental Engineering
Göteborg, Sweden 2006

Bond of corroded reinforcement
Analytical description of the bond-slip response
HENDRIK SCHLUNE
Department of Civil and Environmental Engineering
Division of Structural Engineering
Concrete Structures
Chalmers University of Technology

ABSTRACT

As maintenance and assessment of concrete structures become more and more important, a good understanding of the bond and anchorage behaviour of corroded reinforcement is essential. This master thesis aims to give practical recommendations how to consider the change in bond behaviour for corroded reinforcement by adjusting bond-slip curves for uncorroded reinforcement.

Results from a parameter study done by finite element analyses were analysed to examine the influence of different parameters on the bond behaviour of corroded reinforcement. The parameter study covered different geometries, different bar diameters, different types of concrete and different levels of corrosion penetration. The results were used to develop a method that gives the bond-slip curve of corroded reinforcement if the bond-slip response of uncorroded reinforcement is known. This is done by shifting the bond-slip curve of uncorroded reinforcement along the slip-axis; thus it is possible to obtain the bond-slip response including the maximum bond stress for the corroded reinforcement. The shift along the slip axes is determined by the degree of corrosion. The method is based on the hypothesis that the bond stress is mainly determined by the radial stresses around the reinforcement bar. The method assumes that each geometry has a unique radial stress-radial deformation curve, and that the radial deformations caused by corrosion can be related to the radial deformations caused by slip. The method was also applied on the bond-slip model given in the CEB-FIP Model Code 1990 to extend its area of validity to corroded reinforcement.

The method was shown to be valid for different loading sequences. It was further compared to test results available in literature. With the introduced method it is possible to estimate the influence of corrosion on the bond-slip response, including the bond strength and the dissipated energy.

Key words: corrosion, splitting stresses, bond strength, concrete-cover cracking, steel-concrete interface, pull-out tests, bond, transverse reinforcement, Model Code 1990.

Contents

Preface

This master thesis was carried out from August 2006 to December 2006 at Chalmers university of Technology, at the department of Civil and Environmental Engineering, Division of Structural Engineering, Concrete Structures, Göteborg, Sweden.

At first, I would like to thank my three supervisors Karin Lundgren, Per Kettil and Kamyab Zandi Hanjari for their guidance and support throughout the development of this study. In addition, I would like to thank Armando Soto San Roman who conducted the parameter study that was used as a base for this project and who became a good friend during the last months. I would like to give my appreciation to Fang Sue and Majid Mokabberian for being helpful opponents. I would also like to apologise to Helén Broo and Anette Jansson for taking their software licences.

Furthermore, I would like to thank all the people that made it possible to study here in Sweden and made the last eighteen month to a great experience.

Finally, I dedicate this work to my family, my girlfriend and my friends.

Göteborg, Sweden, December 2006

Hendrik Schlune

Notations

Roman upper case letters

A_s	Area of one reinforcement bar
A_{trans}	Area of transverse reinforcement
D_{11}	Stiffness in the elastic stiffness matrix in normal direction
D_{22}	Stiffness in the elastic stiffness matrix in longitudinal direction
D_{33}	Stiffness in the elastic stiffness matrix in tangential direction
E_s	Young's modulus
F	Dissipated energy
F_n	Normalized dissipated energy
F_1	Yield line describing the friction
F_2	Yield line describing the upper limit at a pull out failure

Roman lower case letters

a	Free increase in the radius of the steel bar
c_{main}	Concrete cover of the main reinforcement
$c_{main,\min}$	Minimum of concrete cover hand half clear bar spacing
c_{trans}	Concrete cover of the transverse reinforcement
d_{main}	Diameter of the main reinforcement
d_{trans}	Diameter of the transverse reinforcement
f	factor to describe the ratio between splitting deformation caused by slip and corrosion
f_{ck}	Characteristic concrete compressive strength
f_{cm}	Mean concrete compressive strength
h	Height
n	Number of bars enclosed by stirrups
s	Slip
s_{conv}	Slip, till where the dissipated energy was calculated
$s_{crack,x}$	Slip that caused a cover crack for a corrosion penetration of x
$s_{crack,eff}$	Effective slip when the first cover crack appears
s_{trans}	Spacing of the transverse reinforcement
th	Thickness
u	Relative displacement across the interface
u_l	Longitudinal displacement, slip
u_{lbond}	Longitudinal displacement in bond layer, slip in the bond layer
u_r	Relative radial displacement at the interface
u_{rbond}	Radial deformation in the bond layer
u_{rcor}	Real increase of the radius of the reinforcement bar due to corrosion
u_{tbond}	Tangential displacement in the bond layer

w	Width, main bar spacing
w_{clear}	Clear main bar spacing
x	Corrosion penetration
x_{crack}	Corrosion penetration when the first crack reaches the surface

Greek upper case letter

Δs_x	Shift of the bond-slip curve for uncorroded reinforcement

Greek lower case letter

φ	Secant stiffness
σ	Stresses at the interface
σ_r	Radial splitting stress
σ_t	Stress in tangential direction
τ	Bond stress

1 Introduction

1.1 Background

Steel-to-concrete bond is a main parameter that influences the structural behaviour of reinforced concrete structures. The transfer of stresses makes it possible to combine the compressive strength of concrete with the tensile strength of steel.

In the past, a lot of research has been made in this field and a wide knowledge has been gained. Less effort has been put into the bond between corroded reinforcement and concrete. During recent years, the durability and sustainability of concrete structures became more and more important. It is commonly assumed that the lifetime is ended when corrosion has been initiated; this leads to large concrete covers. In addition, in many existing structures corrosion has already been detected, see Figure 1.1. By estimating the maximum allowable corrosion in combination with the corrosion rate it is possible to extend the service life over the initiation period into the propagation period.

Figure 1.1 Corroded reinforcement at the Nötesunds Bridge, Sweden

The effect of corrosion on structural integrity is essential to predict the residual strength and the residual lifetime. The steel area decrease is relatively easy to consider while the changed bond properties are usually neglected by those working with assessment and maintenance. This approach can be on the unsafe side; this has been proved by experimental studies, see CEB (2000). The reinforced concrete elements are generally more susceptible to anchorage failure due to reinforcement corrosion than to a decrease in load bearing capacity caused by the reduction in steel area. The interaction between reinforcement and surrounding concrete is decisive for both the load bearing capacity and ductility in the ultimate state, as well as the stiffness and distribution of cracks in the service state. Therefore it is of interest how to consider the changing bond properties depending on the corrosion penetration of the reinforcement bars.

1.2 Aim, Scope and Limitations

The aim of this thesis is to give practical recommendation how to consider the change in bond-behaviour for corroded reinforcement. It should quantify the effect of corrosion penetration for different concrete types and different geometries.

In a first step a parameter study was analysed. The results were used to develop a method to modify bond-slip curves for uncorroded reinforcement to obtain the bond-slip curves for corroded reinforcement. This method was then introduced in the bond-model given in Model Code 1990 to extend it to corroded reinforcement. That should make it possible to predict the mean bond-slip response under various conditions without running a FE-analysis or performing any test.

The work was limited to bond behaviour of ribbed bars. Most results are based on the parameter study carried out by San Roman (2006) and therefore dependent on its correctness and accuracy.

1.3 Method

A parameter study, carried out by San Roman (2006), was analysed to get further knowledge of the bond-slip behaviour of corroded reinforcement. Within this study a simple model that represents a part of a beam or slab has been modelled in the finite element program DIANA. The recorded bond-slip curves together with the crack-pattern were used to investigate how corrosion of the reinforcement bar influenced the bond performance. The effect in bond-strength, dissipated energy and stiffness was quantified depending on the geometry. These results were here used to extend the bond model given in Model Code 1990 to corroded reinforcement. Finally, the drawn conclusions were checked with other reported tests.

2 Description of the Analysed Parameter Study

To get further knowledge of the bond-slip behaviour of corroded reinforcement a parameter study, carried out by San Roman (2006), was analysed. It is shortly described in the following.

2.1 Description of the bond model

The bond model used for the analysed parameter study has been developed and more precisely described by Lundgren (2005a). For the FE-analyses a frictional bond model has been implemented within special interface elements between the reinforcement bars and the concrete. The model is based on the elasto-plastic theory. The steel bar and the surrounding concrete are modelled using solid elements. The interface elements describe the relation between the stresses σ and the relative displacement u in the elastic range according to equation (2.1). The stresses and displacements are defined according to Figure 2.1.

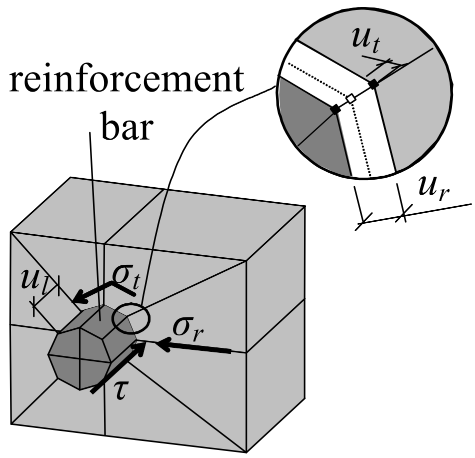

σ_r = radial stress

τ = bond stress

σ_t = tangential stress

u_l = slip

u_r = relative radial displacement in the layer

u_t = tangential displacement

Figure 2.1 Physical interpretation of the variables $\sigma_r, \tau, \sigma_t, u_r, u_l$ and u_t modified from Lundgren (2005a)

$$\begin{bmatrix} \sigma_r \\ \tau \\ \sigma_t \end{bmatrix} = \begin{bmatrix} D_{11} & 0 & 0 \\ 0 & D_{22} & 0 \\ 0 & 0 & D_{33} \end{bmatrix} \begin{bmatrix} u_{rbond} \\ u_{lbond} \\ u_{tbond} \end{bmatrix} \tag{2.1}$$

In equation (2.1), D_{33} prevents the bar from rotating while D_{11} and D_{22} describe the relation between displacements and stresses in radial and transversal direction respectively. The included yield surface is described by two functions. One function describes the friction, F_1, while the other, F_2, describes the upper limit at pull-out failure, see Figure 2.2.

$$F_1 = |\tau| + \mu \cdot \sigma_r = 0 \tag{2.2}$$

$$F_2 = \tau^2 + \sigma_r^2 + c \cdot \sigma_r = 0 \tag{2.3}$$

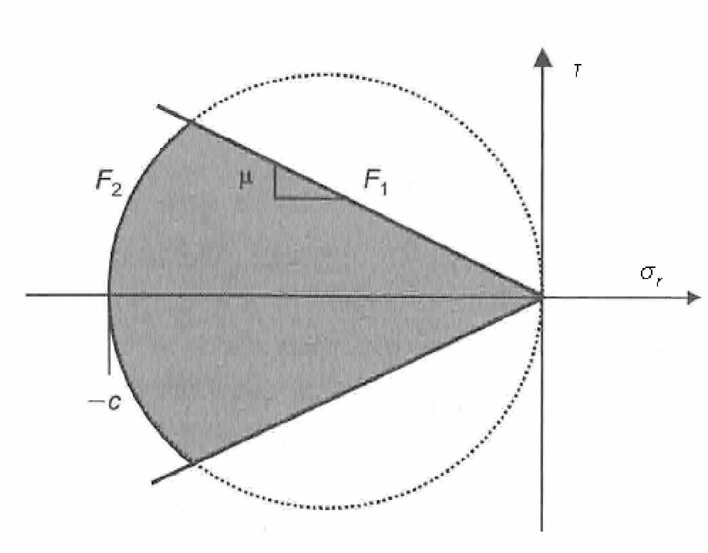

Figure 2.2 The two yield lines, modified from Lundgren (2005a)

In addition, a softening parameter has been established to consider the reduced bond stress for increasing slips due to deterioration of the microstructure. The model has been calibrated for normal strength concrete and reinforcement of type B500B Ø16.

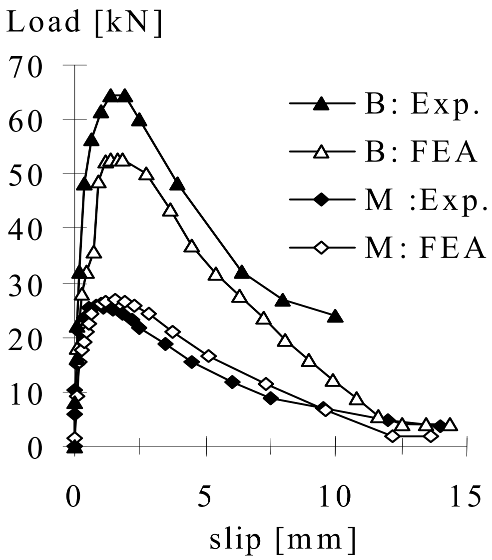

Figure 2.3 Load versus slip in pull-out tests with short embedment length. The experimental results are from Balázs and Koch (1995) and Magnusson (1997), modified from Lundgren (2005a)

The model has been tested for various kinds of pull-out tests. The agreement between results from the analyses and different experiments was rather good, see Figure 2.3. It could be observed that the model is able to predict splitting failure, yielding failure, and to simulate cyclic loading.

2.2 Description of the corrosion model

The corrosion model, which has been used in the analysed parameter study, has been developed by Lundgren (2005b). In this model the increase in volume of corrosion relative to the uncorroded steel, v, is modelled with special interface elements denoted as the corrosion layer. Furthermore, the mechanical behaviour of rust is taken into account.

To explain better the normal stresses produced by corrosion, see Figure 2.4, where the penetration of corrosion is denoted by x, the free increase in the radius of the steel bar is denoted by a (stresses equal to zero) and u_{rcor} is the real increase of the radius of the bar due to restraint forces produced by the surrounding concrete (stresses different from zero).

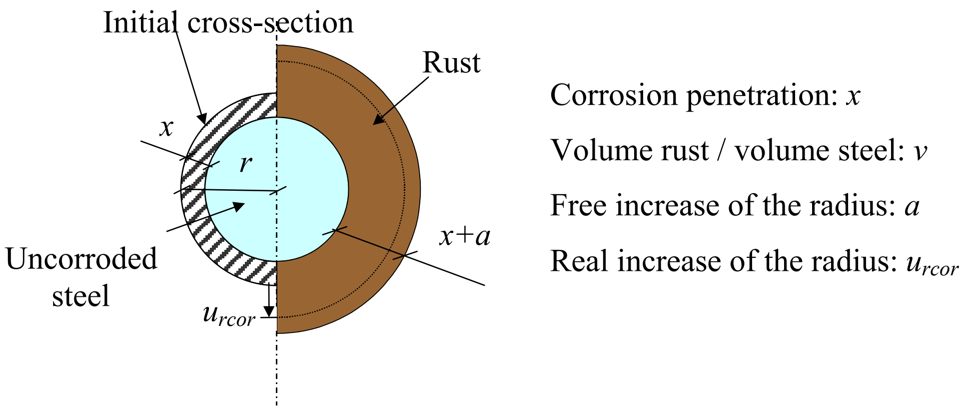

Figure 2.4 Physical interpretation of the variables in the corrosion model modified from Lundgren (2005b)

Few studies have been made to describe the mechanical behaviour of rust. The studies concluded that it behaves as a granular material. The stiffness of the rust varies depending on the stress level and can be described as

$$\sigma_r = K_{cor} \cdot \varepsilon_{cor}^{p} \tag{2.4}$$

where K_{cor} represents the stiffness of the corrosion products in radial direction, ε_{cor} represents the strain in the rust and p is an exponent to describe the granular behaviour.

The corrosion model has been combined by Lundgren with the bond model described in section 2.1 considering the corrosion effect as an increase of volume in the steel bar. The effect in frictional behaviour between reinforcement and concrete is taken into account introducing a function $k\left(\frac{x}{r}\right)$ in the friction coefficient equation

$$\mu(\kappa) = k\left(\frac{x}{r}\right) \cdot \mu_0(\kappa), \qquad but \quad \mu(\kappa) \geq 0.4 \tag{2.5}$$

where $\mu_0(\kappa)$ is the friction coefficient for uncorroded reinforcement.

Values of $k\left(\frac{x}{r}\right)$ are given in Figure 2.5.

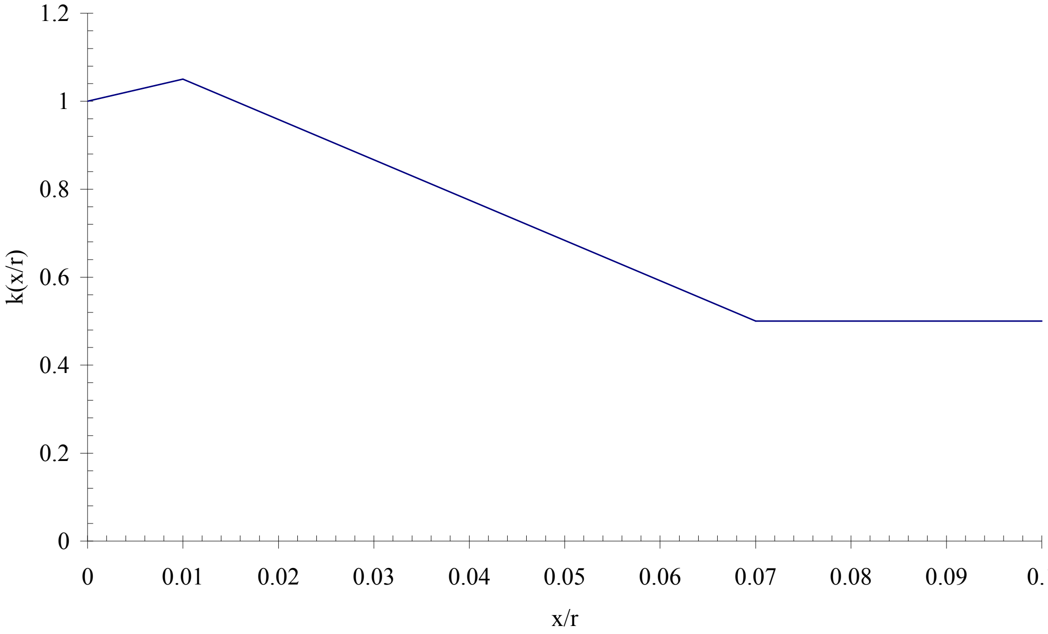

Figure 2.5 *Function* $k\left(\frac{x}{r}\right)$ *versus corrosion penetration – reinforcement radius ratio.*

2.3 FE-model

2.3.1 Geometry

The different analysed geometries have been chosen to represent a part of a reinforced concrete slab or beam. A mean geometry has been defined and parameters have been varied according to Figure 2.7. For the mean geometry a spacing of the main reinforcement bars of $w = 100$ mm has been assumed. A concrete cover of $c_{main} = 30$ mm related to the main reinforcement has been chosen. The transverse reinforcement had a diameter of $d_{trans} = 10$ mm and a spacing of $s_{trans} = 300$ mm. That led to a concrete cover of $c_{trans} = 20$ mm for the transverse reinforcement. A concrete type C40 has been chosen. The mean geometry is shown in Figure 2.6.

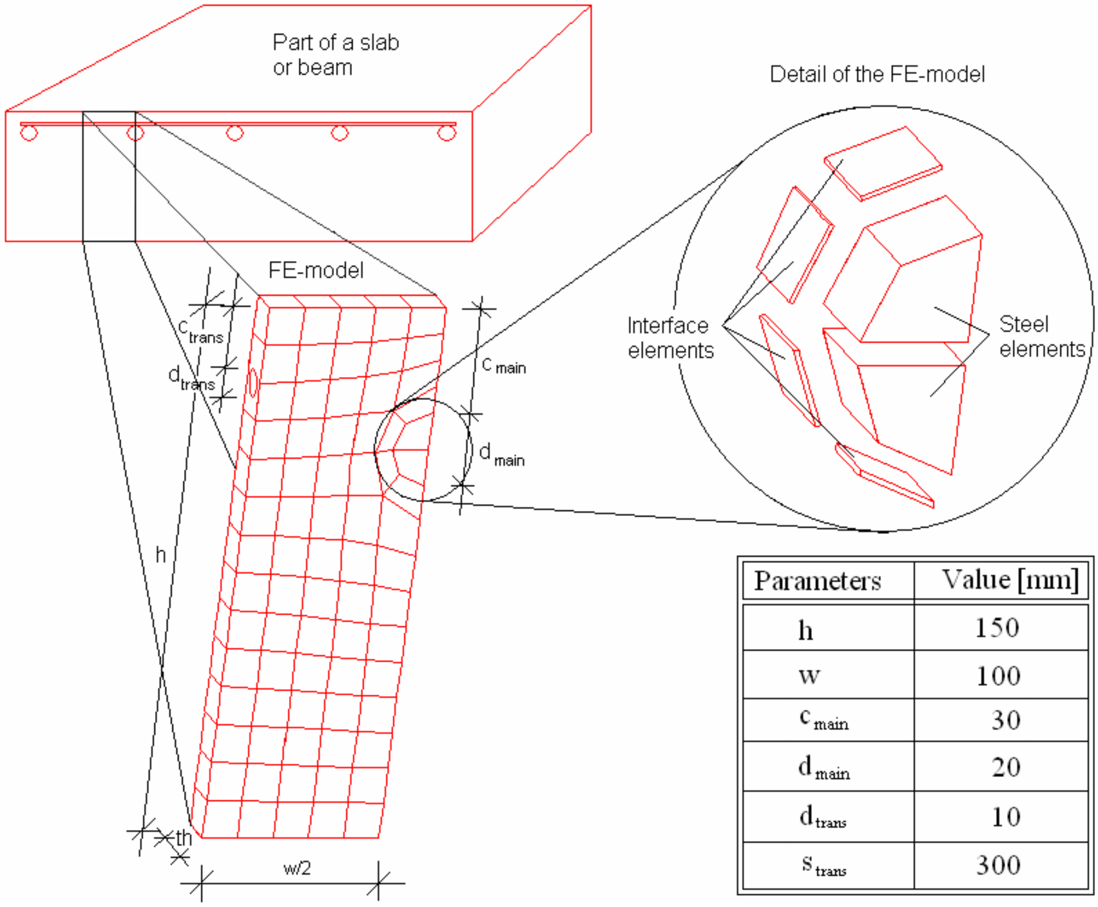

Parameters	Value [mm]
h	150
w	100
c_{main}	30
d_{main}	20
d_{trans}	10
s_{trans}	300

Figure 2.6 Geometry (values for mean geometry are defined in the table)

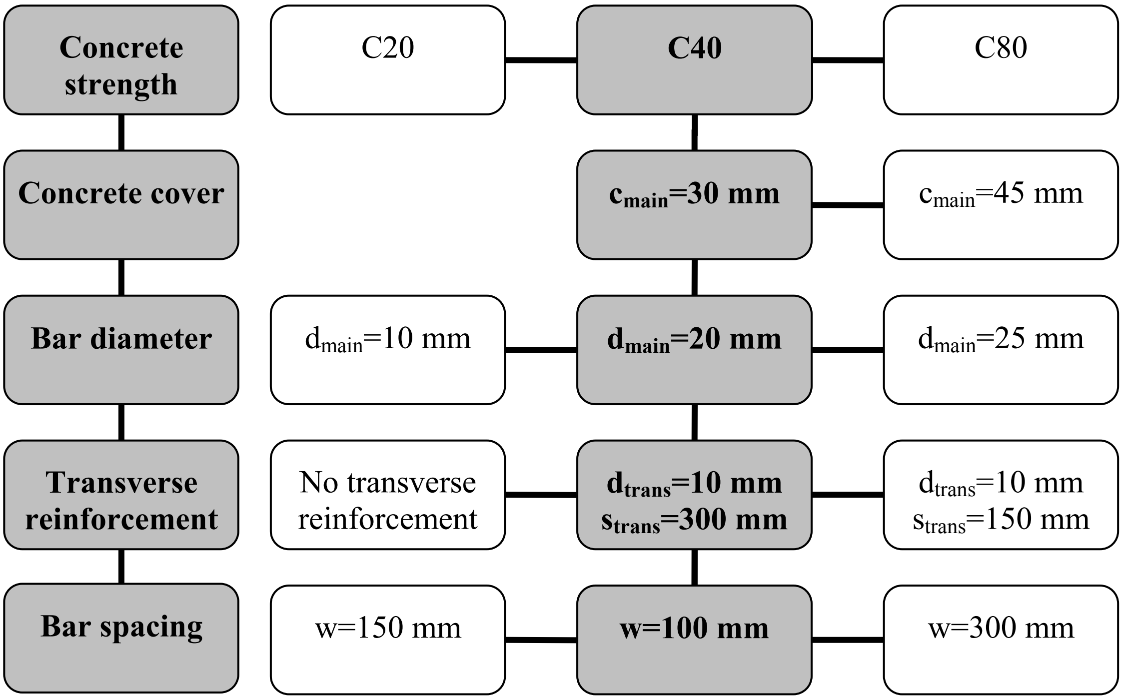

Figure 2.7 Analyses scheme (mean geometry is marked grey)

2.3.2 Material Data

Different concrete types have been used in the parameter study to study the effect of the concrete strength on the bond behaviour of corroded reinforcement. All values were mean values according CEB-FIP Model Code 1990 for a maximum aggregate size $d_{\max} = 16$ mm. These values only differ marginally from values according to EC 2.

The reinforcement steel has been modelled as ribbed bars with three different diameters $d_{main,1} = 10$ mm, $d_{main,2} = 20$ mm and $d_{main,3} = 25$ mm. As the expected stresses have been assumed to be lower than the yield stress, a linear elastic model with a modulus of elasticity of $E_s = 200$ GPa has been chosen.

2.3.3 Loading

The loading consisted of two phases. In the first phase the corrosion has been applied in 50 steps. The step size depended on the final corrosion penetration that varied between $x = 0$ µm and $x = 200$ µm. In the second phase the reinforcement bar has been subjected to a pull-out load in 400 steps with the step size of 0.005 mm. That led to a total pull-out displacement of 2 mm.

2.3.4 Boundary conditions

In the x-y-plane, the right boundary translation has been restrained in x direction. The left hand side has been restrained to remain as a straight line and able to rotate around the z-axis. Finally, translations in y direction have been restrained in the longitudinal mid-plane of the steel elements. The last restraint that has been used is shown in Figure 2.8 (b) where the back surface corresponding to the x-y-plane of the model has not been allowed to move in z direction.

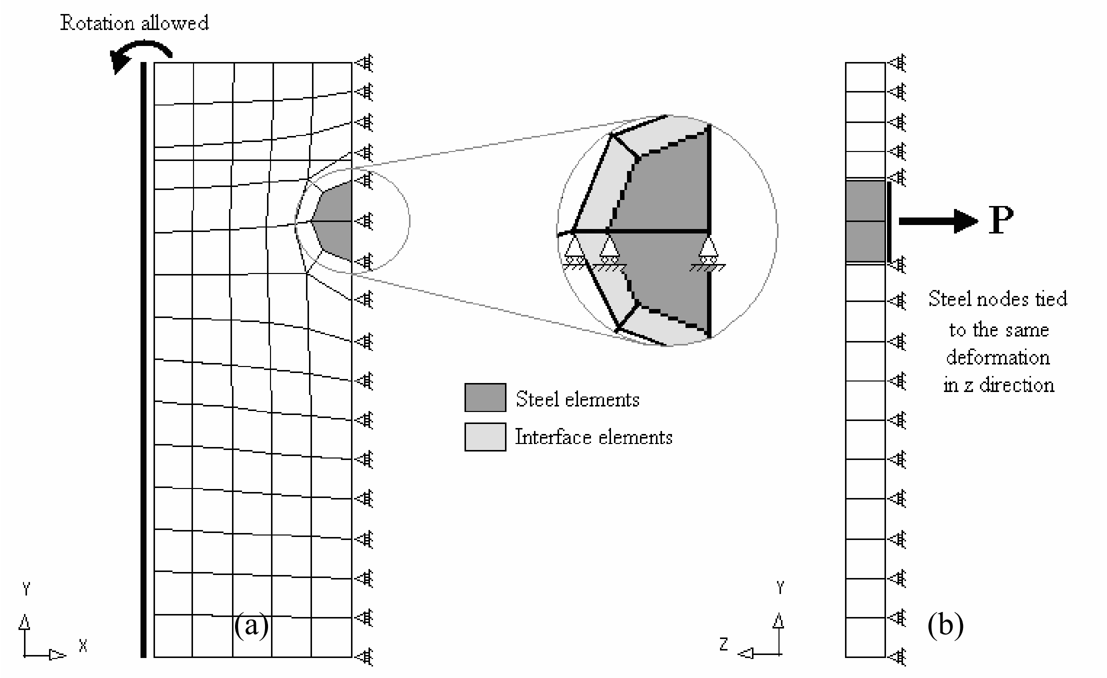

Figure 2.8 Boundary conditions in different planes (a) x-y-plane (b) z-y-plane

2.3.5 Limitations

First of all it should be stated that the parameter study only varied some parameters while others have been left without consideration. The influence of transverse pressure and the loading history are only two important parameters, besides others, that were not taken into account. In addition the results were based on only a few variations of each parameter. As mainly one parameter at the time has been varied the interaction of the parameters was difficult to observe. The analysed geometry represented only a small part of the slab or the beam. The transverse reinforcement has only been modelled as embedded reinforcement along a line perpendicular to the main reinforcement bar. Therefore it was not possible to consider the influence of closed stirrups on the confinement. Corrosion of the transverse reinforcement has not been considered.

As the parameter study has been conducted by using FE-analysis instead of performing tests, some more limitations have to be considered. The used bond and corrosion models have mainly shown good agreement with tests. Even so the accuracy should not be overestimated. For more information of the precision see Lundgren (2005a) and Lundgren (2005b). As the analysed structure showed brittle behaviour, some analyses did not converge. Especially the results for the post cracking behaviour were mesh and load step dependent. After cracks had separated the specimen into two pieces, the results were not reliable anymore.

2.3.6 Results

The results of the parameter study have been reported in San Roman (2006). Bond-slip curves have been presented together with the obtained crack-pattern. The stresses of the transverse reinforcement have been checked for some specimens. In addition access to all output files has been provided by San Roman to get further insight of the structural behaviour of the specimens.

The most important data are summarized in Appendix A.

3 Evaluation of the Results

In addition to the bond-slip curves reported by San Roman (2006), the crack pattern and the stresses and strains were used to analyze the results.

3.1 General results

The slip and the corrosion cause splitting deformation that can cause splitting cracks. The point when the first crack reached the surface turned out to limit the bond stress and gave a change in the bond stiffness. For uncracked specimens the bond strength decreased by less than 15% due to corrosion. When the applied corrosion cracked the cover before the pull-out was applied, a much higher influence of the corrosion on bond-strength can be observed. Therefore, an analytical equation was developed to predict that point, see Chapter 3.6. The bond stiffness development is described in Chapter 3.7. To explain the influence of corrosion on bond strength and the dissipated energy, a distinction between four different cracking modes was introduced, see Figure 3.1. The dissipated energy is in the following defined as the area under the bond-slip curve. As some analyses did not converge the calculated area was limited to the slip, s_{conv}, until which most analyses showed convergence; see Appendix A.

The crack pattern was mainly influenced by the cover to clear bar spacing ratio. For a concrete cover to clear bar spacing ratio of $c_{main}/w_{clear} \geq 0.5$ the specimens developed first a horizontal crack. This cracking mode will in the following be called "cracking mode 1", see Figure 3.1(1). For a ratio of the concrete cover to the clear bar spacing between 0.5 and 0.375 the first crack developed vertically. The second crack developed horizontally; see Figure 3.1(2). This cracking mode will in the following be called "cracking mode 2". For wide specimens with a concrete cover to clear bar spacing ratios smaller or equal to 0.375 the first crack again developed vertically while the second crack developed inclined to the same surface, see Figure 3.1(3). This cracking mode will in the following be called "cracking mode 3". In wider cases without transverse reinforcement the first crack reached the top surface and the second crack developed vertically to the bottom surface. This will be called "cracking mode 4".

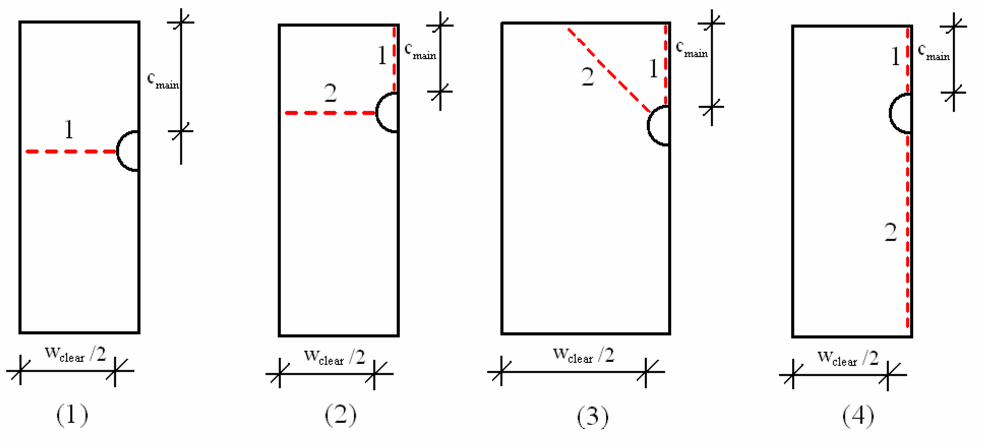

Figure 3.1 Cracking modes

3.2 Cracking mode 1

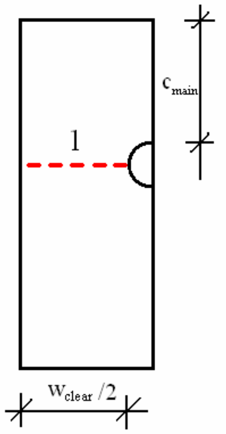

Figure 3.2 Crack pattern for cracking mode 1

For specimens with a concrete cover larger than half the clear bar spacing the specimens developed a horizontal crack to the side surface. In this case the specimens were suddenly separated into two pieces. The confinement was lost and the bond stress dropped to a very small residual value, see Figure 3.3. If the crack reached the surface by only applying the corrosion almost no bond stress developed when the reinforcement bar was pulled out, see Figure 3.4. Therefore the corrosion had a major influence on the dissipated energy when it led to a cover crack, see Figure 3.5. When this cracking mode developed, the transverse reinforcement had no favorable effect. How closed stirrups would have influenced the residual bond strength has not been included in the study.

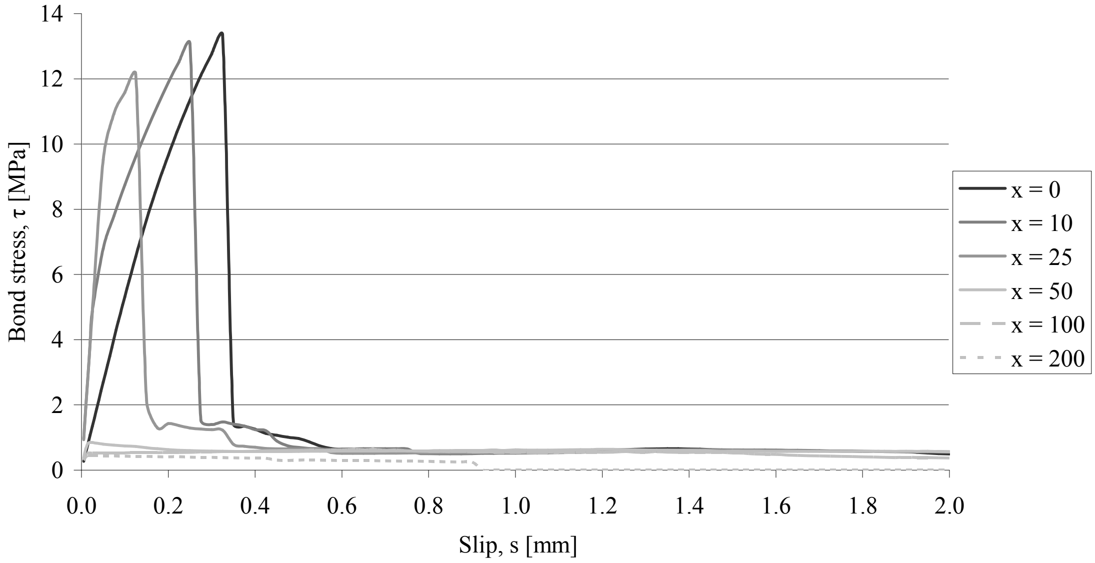

Figure 3.3 Typical bond slip curves for cracking mode 1 (c=45)

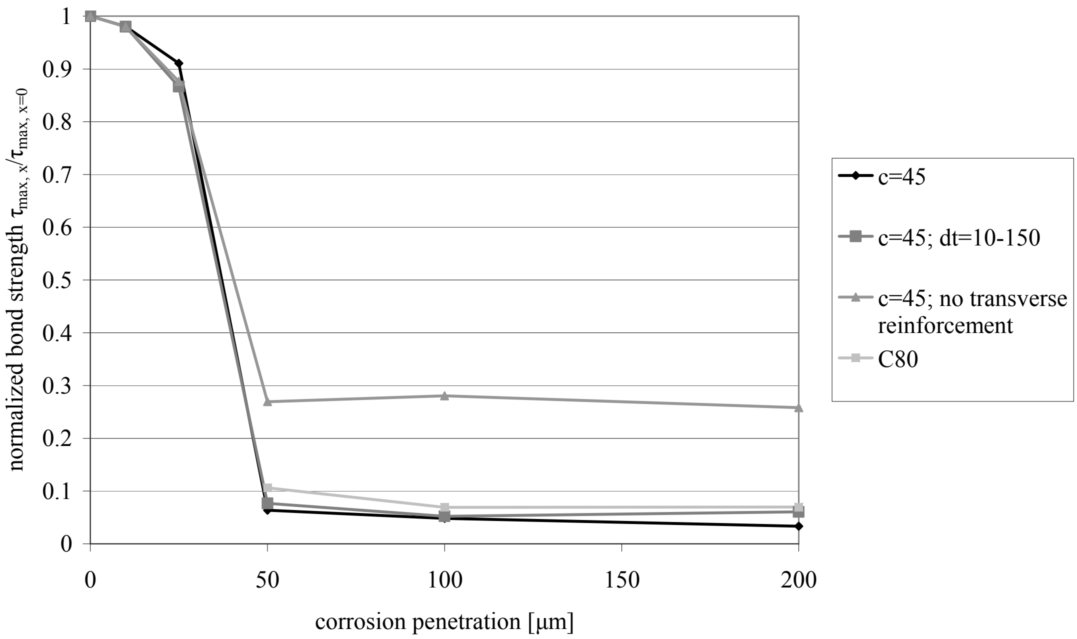

Figure 3.4 Development of the bond strength over the corrosion penetration for specimens with cracking mode 1

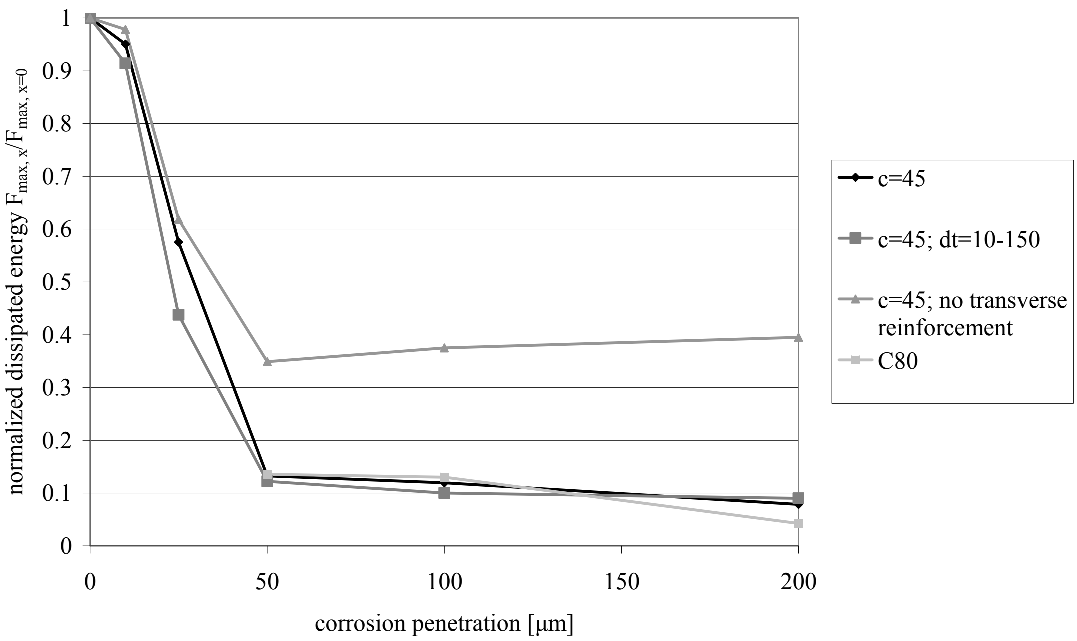

Figure 3.5 *Development of the dissipated energy over the corrosion penetration for specimens with cracking mode 1*

3.3 Cracking mode 2

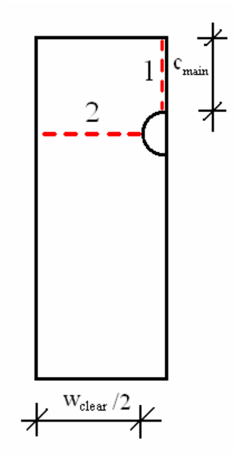

Figure 3.6 *Crack pattern of cracking mode 2*

For specimens with an intermediate ratio between the bar spacing and the concrete cover, the first crack emerged vertical to the upper surface. The second crack developed horizontally to the side. After the first crack developed to the surface, the bond stress decreased to a certain value depending on the amount of transverse reinforcement. As the transverse reinforcement limited the opening of the crack the bond stress stayed almost constant until the horizontal crack reached the surface, see Figure 3.7. For higher amounts of transverse reinforcement the horizontal crack developed faster as the bond stress and the splitting stress stayed on a higher level after the first crack had developed. When the corrosion caused the first vertical cover crack before the pull out was applied, the bond strength did not reach the maximum value of the uncorroded case. When the corrosion caused also the second cover crack almost no bond stress could develop, see Figure 3.8. The sudden drop of the bond stress and the dissipated energy is now delayed to the development of the second crack, see Figure 3.9.

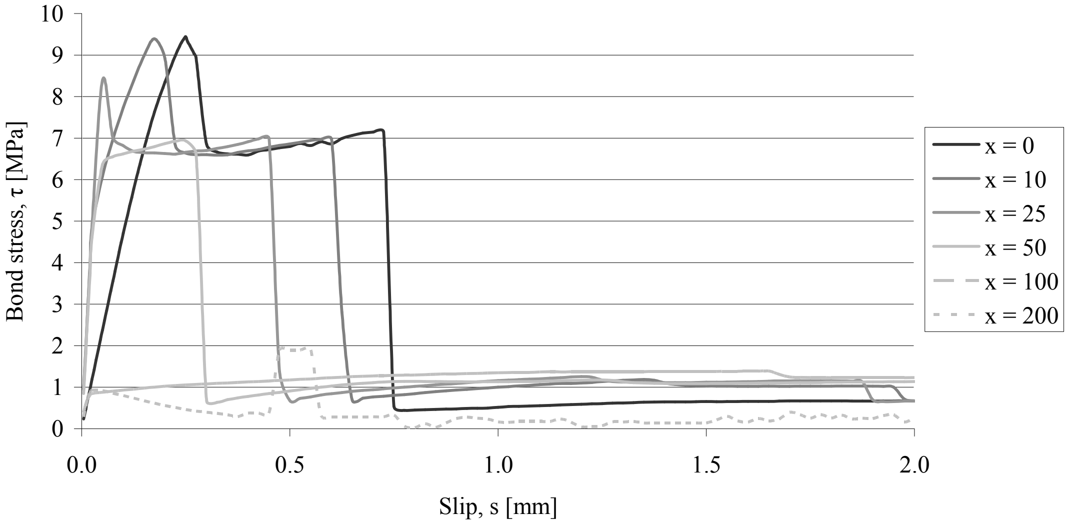

Figure 3.7 Typical bond slip curves for cracking mode 2 (d=25)

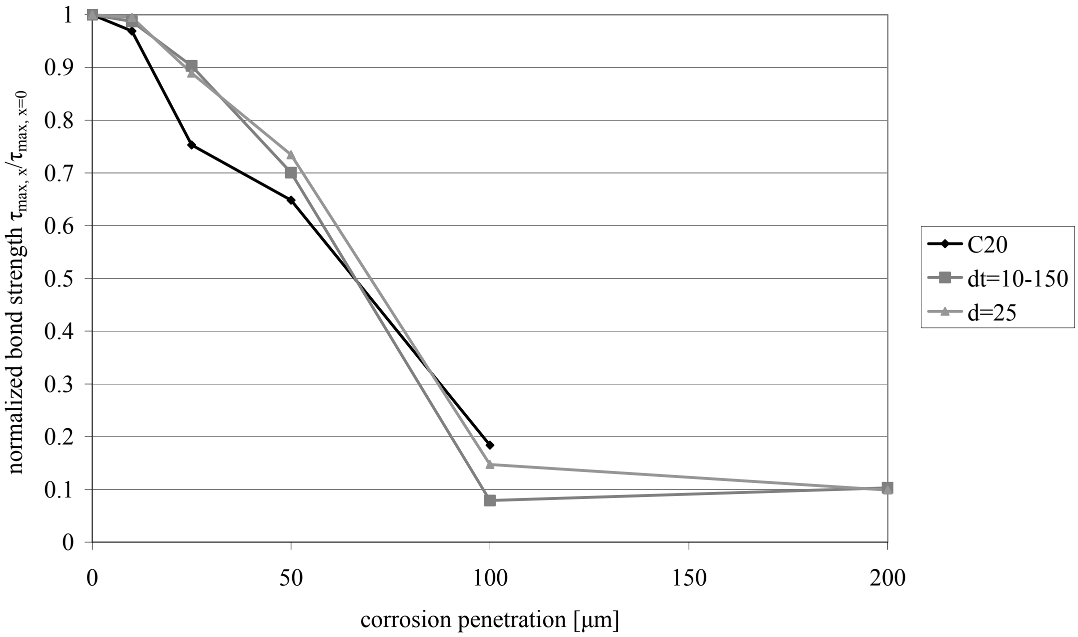

Figure 3.8 Development of the bond strength over the corrosion penetration for cracking mode 2

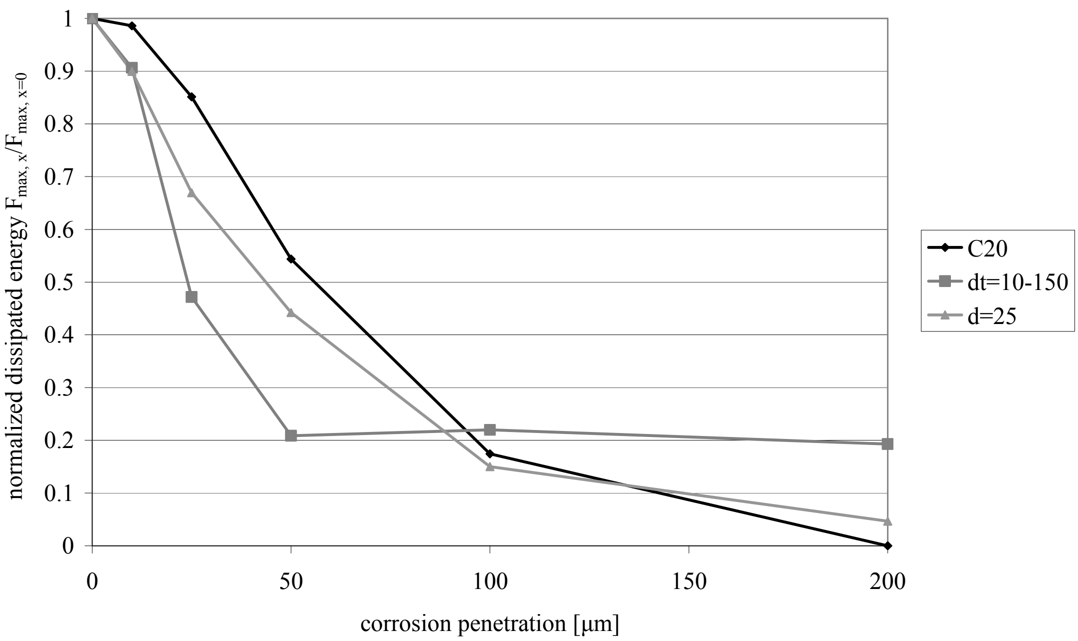

Figure 3.9 Development of the dissipated energy over the corrosion penetration for specimens with cracking mode 2

3.4 Cracking mode 3

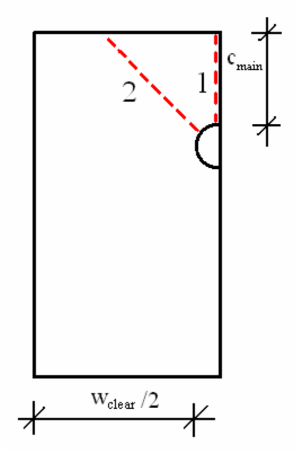

Figure 3.10 Crack pattern of cracking mode 3

For large bar spacing the first crack developed to the upper surface. For increasing radial stresses the second crack emerged inclined to the same surface. After the first cover crack the bond stress decreased. Then the second crack propagated. As the second crack passed the reinforcement no sudden drop of the radial stresses was obtained, see Figures 3.11-3.12. Instead the crack opened slowly with increasing load and the bond stress decreased concurrently. Therefore the development of the dissipated energy was less critical than for the other cracking modes, see Figure 3.13. When the same specimens were tested without transverse reinforcement failure mode 4 occurred.

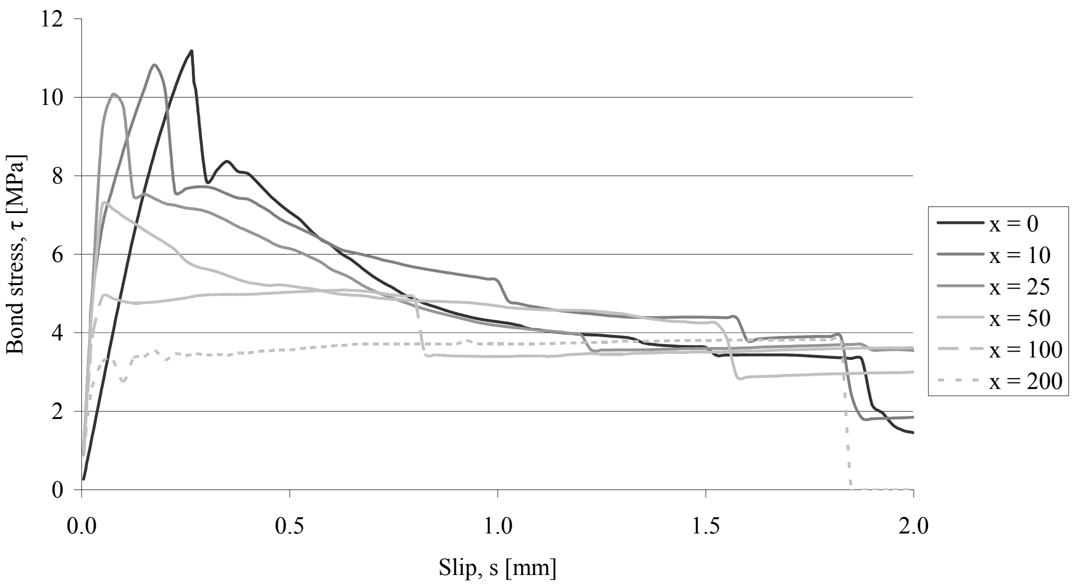

Figure 3.11 Typical bond slip curves for cracking mode 3(w=75)

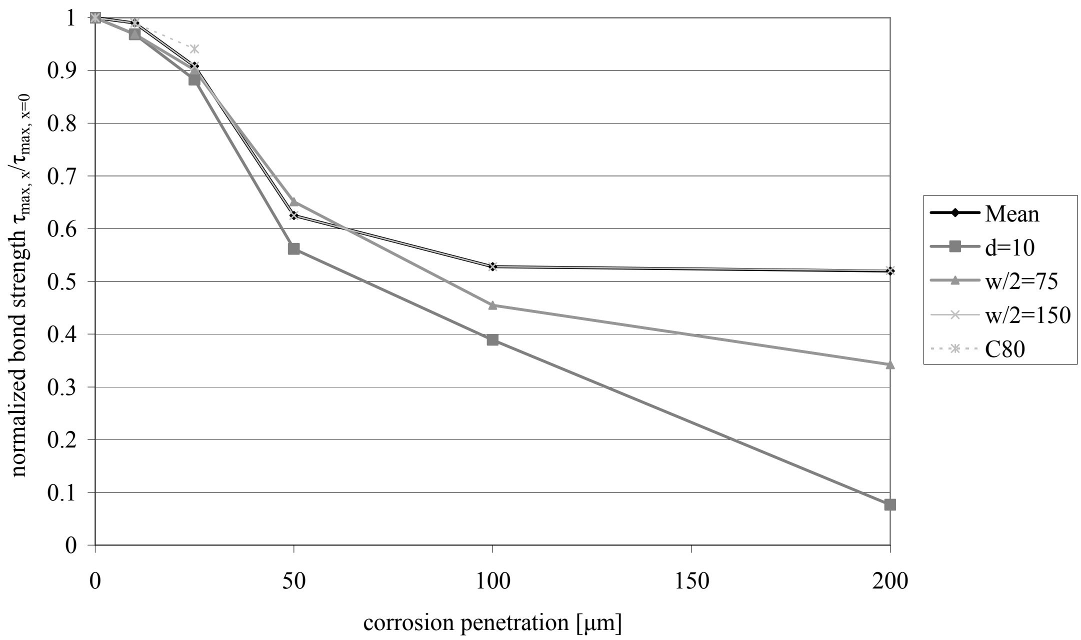

Figure 3.12 Development of the bond strength over the corrosion penetration for cracking mode 3

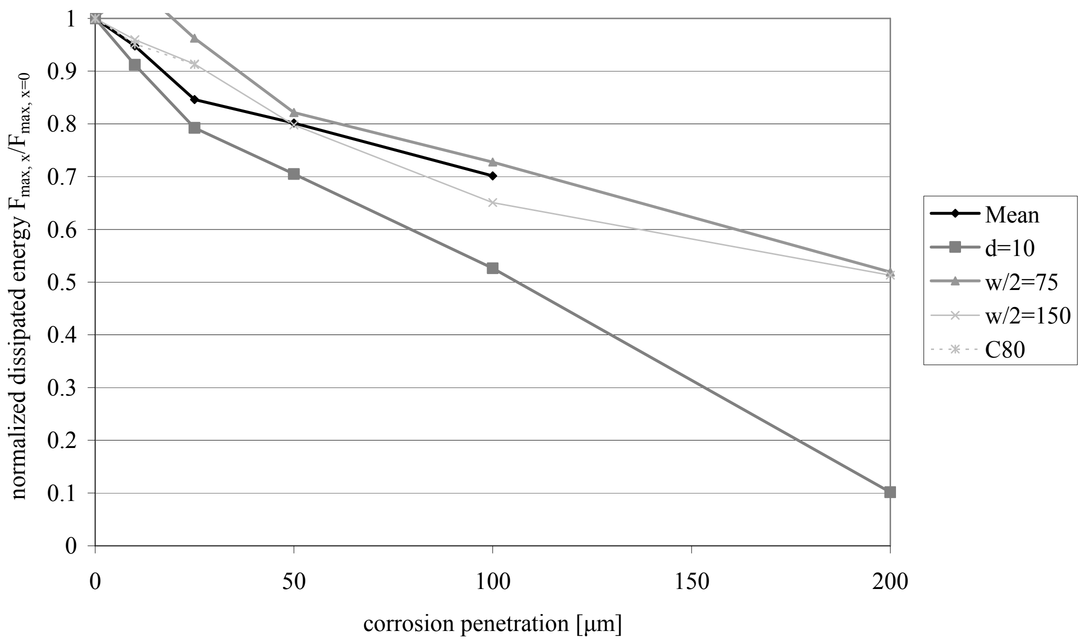

Figure 3.13 Development of the dissipated energy over the corrosion penetration for cracking mode 3

3.5 Cracking mode 4

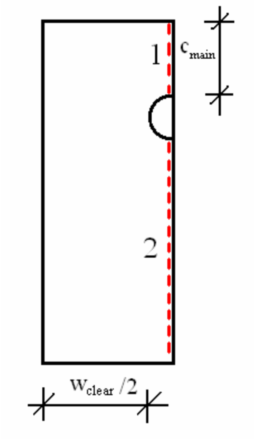

Figure 3.14 Crack patter of cracking mode 4

For the specimen without transverse reinforcement and a cover to clear bar spacing ratio of $c_{main} / w_{clear} < 0.5$ the first crack reached the upper surface. The second crack propagated vertically to the lower surface and separated the specimen. The second crack developed slowly through the specimen so that a certain resistance remained until the crack finally separated the specimen.

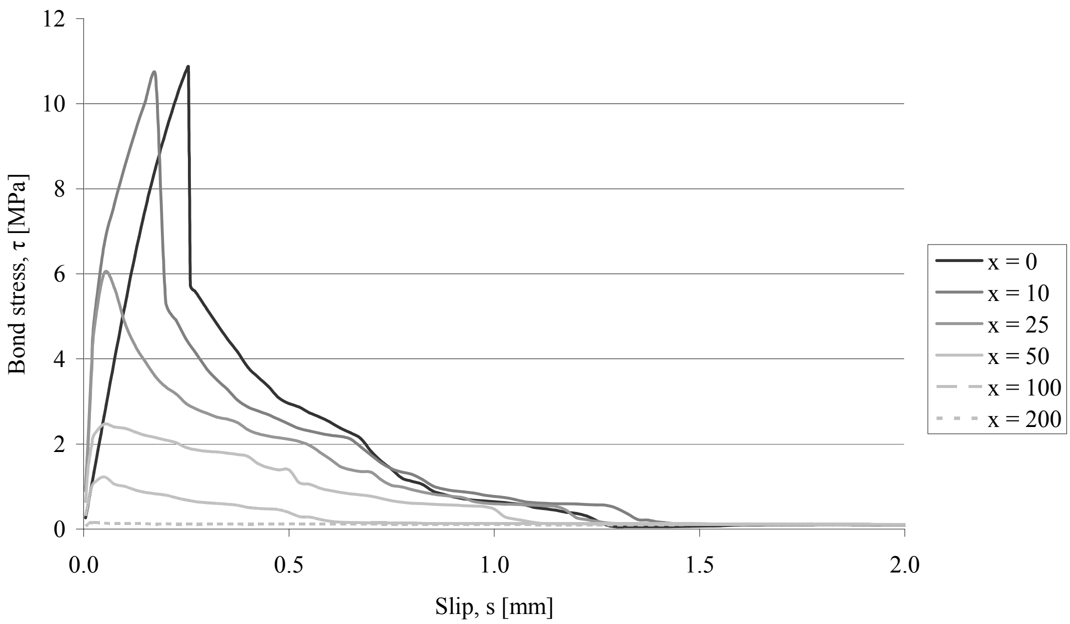

Figure 3.15 Typical bond slip curves for cracking mode 4 (no transverse reinforcement)

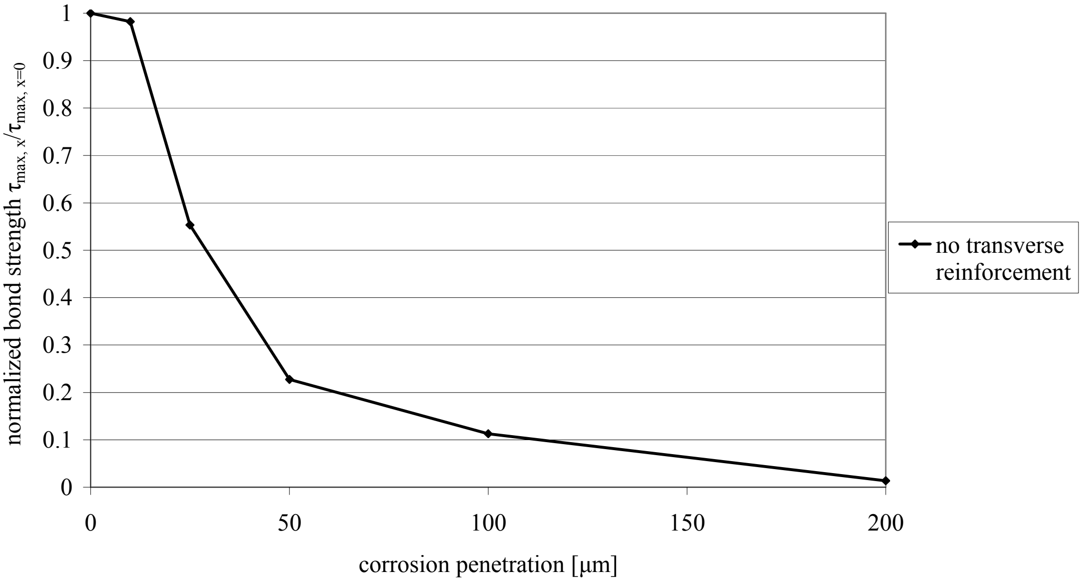

Figure 3.16 Development of the bond strength over the corrosion penetration for cracking mode 4

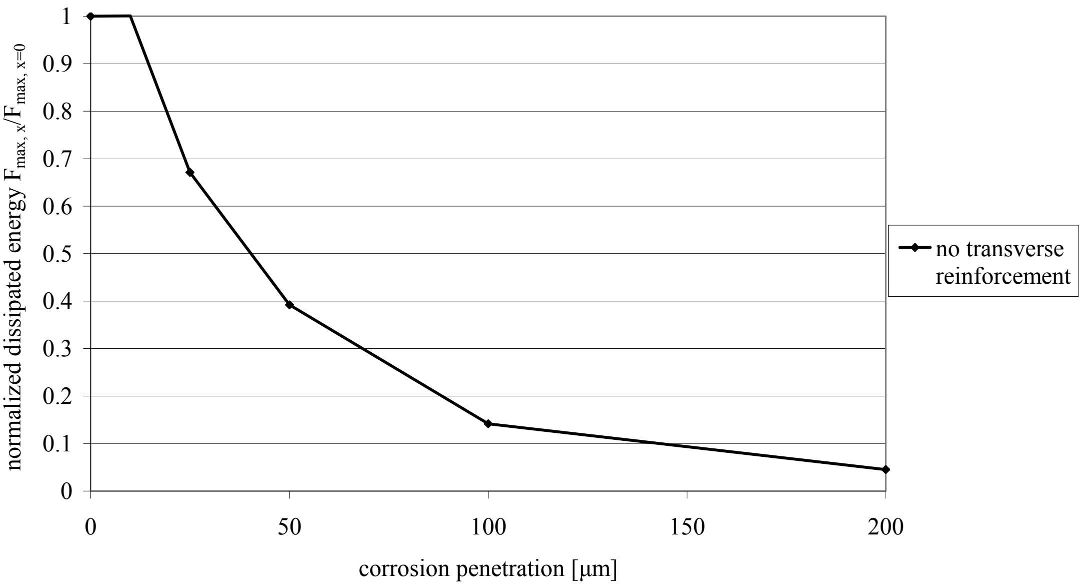

Figure 3.17 Development of the dissipated energy over the corrosion penetration for cracking mode 4

3.6 First cover crack

When the first crack reached the surface the concrete can not resist the tensile ring stresses anymore, which are needed to counteract the splitting stresses, see Figure 3.18. Just before that, the maximum bond stress was obtained. In addition, the development of the first cover crack had influence on the stiffness development. The cover crack can be caused by corrosion, by slip or a combination of both.

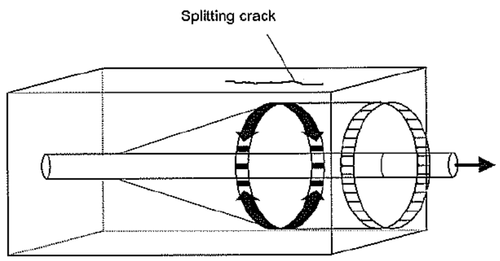

Figure 3.18 Tensile ring stresses in the anchorage zone, according to Tepfers (1973)

3.6.1 Cover crack due to corrosion

Corrosion penetrations between 20 and 45 μm without any pullout led to a crack that reached the surface. A best subset regression analyses was performed to identify the most important predictors to describe for which corrosion penetration the cover cracked. It turned out that a model using two factors already gave good prediction for the parameter study, see Figure 3.19. The chosen predictors were cover-to-diameter ratio and the concrete strength and led to the following equation:

$$x_{crack} = \left(9.13 \cdot \frac{c_{main,\min}}{d_{main}} + 0.313 \cdot f_{cm} \right) \cdot 10^{-3} \qquad (3.1)$$

where

x_{crack} is the corrosion penetration for which the first crack reaches the surface (in mm)

$c_{main,\min}$ is the minimum of the concrete cover and the half clear bar spacing (in mm)

d_{main} is the diameter of the main transverse reinforcement bar (in mm)

$f_{cm} = f_{ck} + 8MPa$ is the mean concrete compressive strength (in MPa)

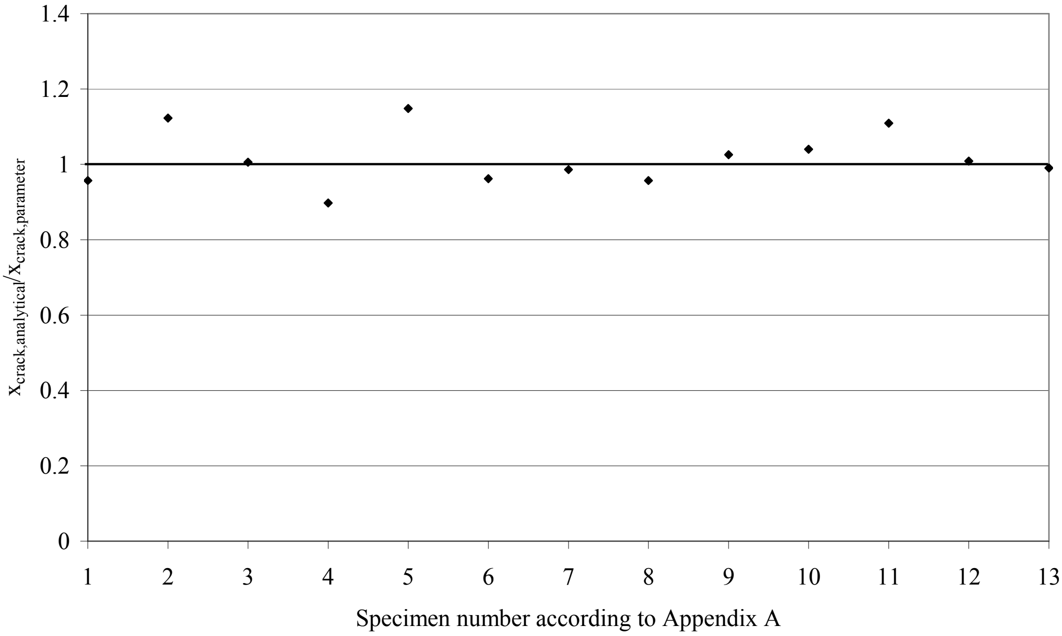

Figure 3.19 Comparison of x_{crack} according to equation (3.1) and according to the parameter study

The transverse reinforcement appeared to be the third most important factor. Its influence on the appearance of the first cover crack was not as high as the effect of the cover-to-bar diameter ratio and the concrete strength. Hence it has not been considered in the empirical expression. The transverse reinforcement became more important after the crack had developed to limit the crack width.

Equation (3.1) was compared with test results from several researchers. The analytical corrosion penetration at cracking divided by the corrosion penetration at cracking measured in the experiments was plotted versus the cover-to-bar ratio, see Figure 3.20. It is obvious that the obtained results are not satisfactory. For smaller cover-to-bar ratios, equation (3.1) overestimates the corrosion that is needed to crack the cover. For higher cover-to-bar ratios the opposite occurs. That led to the conclusion that the effect of the cover-to-bar ratio was underestimated.

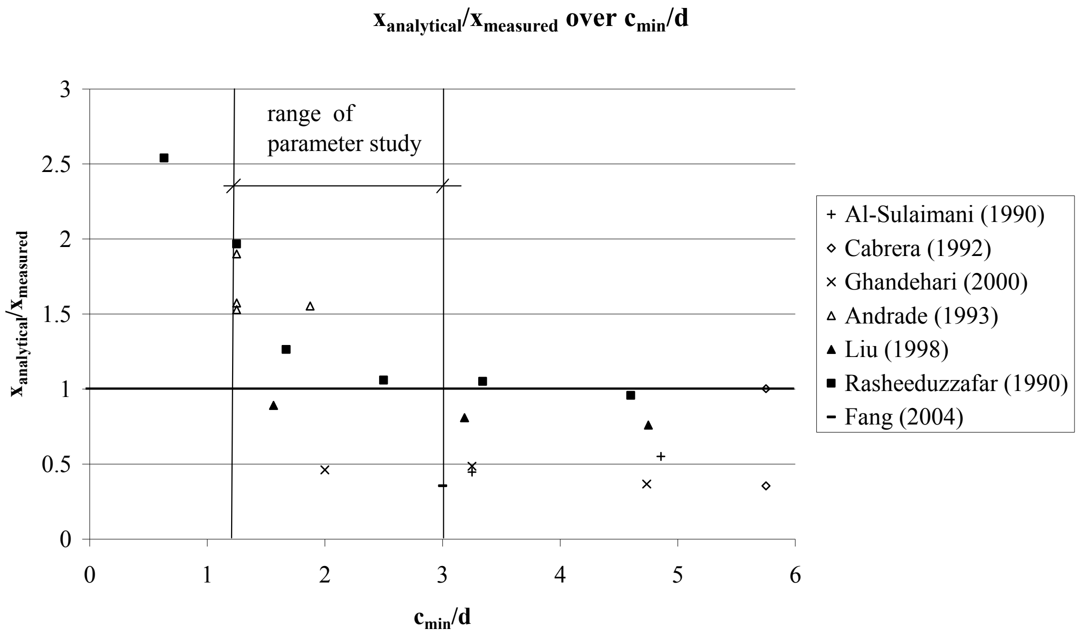

Figure 3.20 Comparison of measured and calculated corrosion penetration according to equation (3.1) that led to cover cracking

As the equation obtained from the parameter study did not lead to feasible prediction for the reported tests, the test results were used to obtain an empirical equation. In a first step the most important predictors were analysed. Possible predictors were $c_{main,min}/d$, $(c_{main,min}/d)^2$, f_{cm} and $\sqrt{f_{cm}}$. An equation using $c_{main,min}/d$ as the only predictor was chosen. It led to the following expression:

$$x_{crack} = \left(20.9\frac{c_{main,\min}}{d_{main}}\right)\cdot 10^{-3} \tag{3.2}$$

The agreement with the test results is now better as before, but still not satisfactory; see Figure 3.21.

The influence of the concrete strength was left without consideration in equation (3.2). It turned out that the effect of the concrete strength was dependent on the considered tests. When tests performed by Fang (2004) were not considered the concrete strength had a negative effect on the corrosion penetration at cracking. By taking Fang's test results into account the opposite occurred. The effect of the concrete strength was in both cases much smaller than the cover-to-bar diameter ratio. It is surprising that the effect of the concrete strength and the concrete tensile strength are almost negligible in the analysed tests. One explanation might be that the effect of the concrete type is overshadowed by other factors that were not taken into account in the empirical formula. Another explanation might be that the higher tensile capacity of higher strength concrete is compensated by higher radial stresses caused by corrosion in higher strength concrete. As higher strength concrete is more compact it can be assumed that a volume expansion of the corrosion products leads to higher radial stresses as the corrosion products have less free volume to penetrate in.

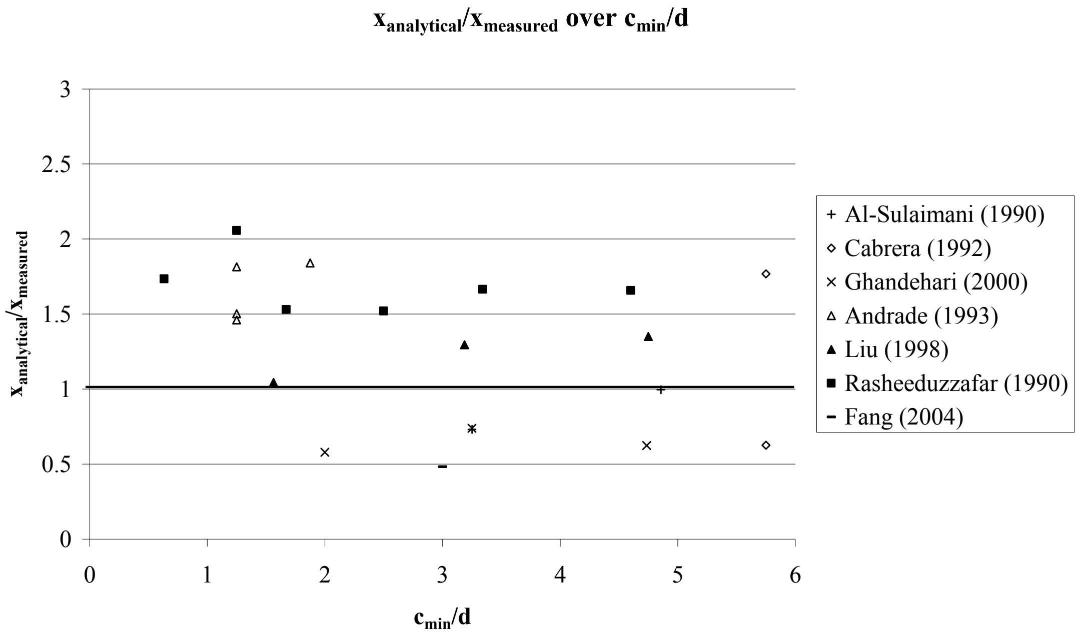

Figure 3.21 Comparison of measured and calculated corrosion penetration according to equation (3.2) that led to cover cracking

3.6.2 Cover crack due to slip

For uncorroded specimens, an active slip between 0.19 mm and 0.375 mm caused a cover crack. Again a best subset regression analyses was performed to identify the most important predictors to describe for which slip the cover cracked. It turned out, that now the bar diameter was more important than for corrosion induced cracking, while the influence of the transverse reinforcement decreased. Besides that, the cover-to-bar diameter ratio was again the most important factor.

3.6.3 Cover crack due to slip and corrosion

The parameter study showed that corrosion decreased the slip that was needed to crack the cover. That is due to the fact that both corrosion and slip cause splitting deformations and this is in good agreement with reported tests, see e.g. Auyeung (2000). It was assumed that there is a specific factor, *f*, to describe the ratio between the splitting deformation caused by slip and corrosion. By comparing the uncorroded case with the case for different corrosion penetrations, equation (3.3) was obtained.

$$s_{crack,x=0} = s_{crack,x} + x \cdot f \tag{3.3}$$

$$\Rightarrow f = \frac{s_{crack,x=0} - s_{crack,x}}{x} \tag{3.4}$$

where

$s_{crack,x=0}$ slip that caused a cover crack for uncorroded reinforcement (in mm)

$s_{crack,x}$ slip that caused a cover crack for a corrosion penetration of x (in mm)

x corrosion penetration (in mm)

f factor to describe the ratio between splitting deformation caused by slip and corrosion

Equation 3.4 was applied for all different geometries of the parameter study and a mean value of $f = 8.1$ with standard deviation of 1.7 was obtained; see Appendix A, column 17. Using this factor, *f*, an effective slip that caused cracking was calculated according to equation (3.5), that takes into account the splitting stresses caused by corrosion.

$$s_{crack,eff} = s_{crack,x} + f \cdot x \qquad (3.5)$$

where

$s_{crack,eff}$ is the effective slip when the first cover crack appears (in mm)

$s_{crack,x}$ slip that caused a cover crack for a corrosion penetration of x (in mm)

f factor to describe the ratio between splitting deformation caused by slip and corrosion

x corrosion penetration (in mm)

It can be seen, that $s_{crack,eff}$ is almost constant for the each geometry, see Figure 3.22. Therefore it can be concluded that the introduced effective slip is an appropriate factor to consider the effect of corrosion on cracking.

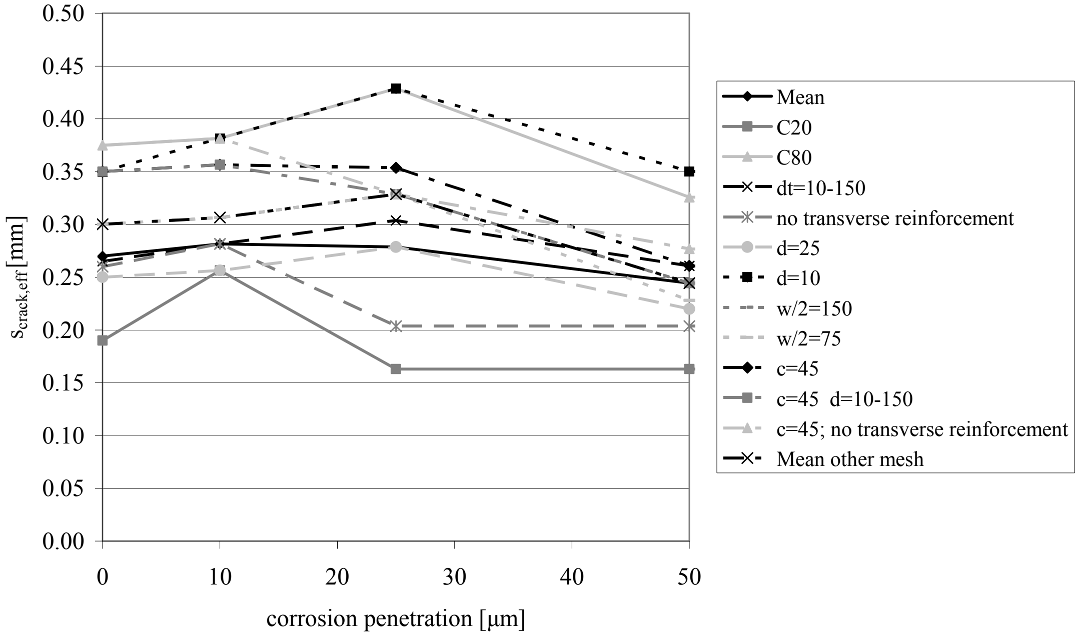

Figure 3.22 Effective slip when the first cover crack appeared according to equation (3.5) over the corrosion penetration

This observation makes it possible to predict the slip at cracking for corroded reinforcement when the slip at cracking is know for the uncorroded case, according to equation (3.6).

$$s_{crack,x} = s_{crack,x=0} - f \cdot x \tag{3.6}$$

where

$s_{crack,x}$	slip that caused a cover crack for reinforcement with a corrosion penetration of x (in mm)
$s_{crack,x=0}$	slip that cause a cover crack for uncorroded reinforcement
f	factor to describe the ratio between splitting deformation caused by slip and corrosion
x	corrosion penetration of the corroded reinforcement (in mm)

3.7 Stiffness development

Corrosion decreases the slip for which the maximum bond stress and the first cover crack develops. As the bond strength decreased less than the slip for which the maximum bond stress is obtained, it can be said that the stiffness of the bond increases considerably for the uncracked state. The slope of a line, from the root of the coordinate system to the maximum bond stress, was calculated. This slope, representing a secant stiffness, was compared for different corrosion penetrations; see Figure 3.23.

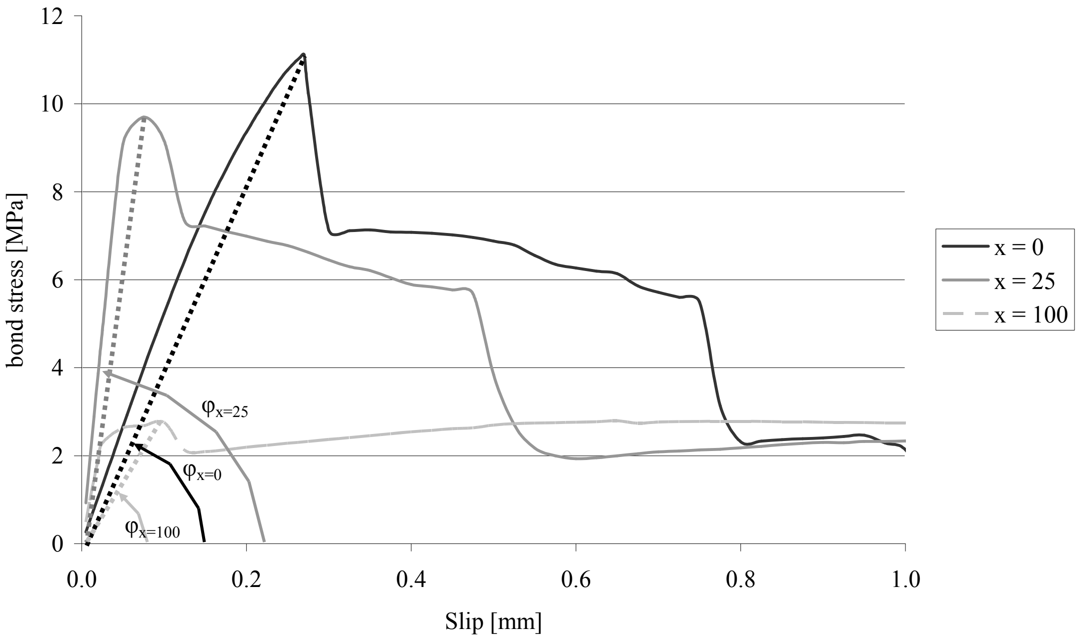

Figure 3.23 Bond stiffness variation due to reinforcement corrosion (Mean, different mesh)

It could be observed that the slope increased for higher corrosion penetration up to the amount of corrosion that led to the first cover crack. When the cover cracked, the stiffness rapidly decreased. The slope of each secant was divided by the slope of the related uncorroded case. In addition, for each specimen the corrosion penetration was divided by the corrosion penetration that led to the first surface crack. In Figure 3.24 the obtained results are summarized. In a final step two best fitting graphs were drawn. One describes the stiffness increase before cracking and the other one describes the stiffness decrease after cracking. Due to the large scatter of the secant stiffness after cracking these results should be handled with caution.

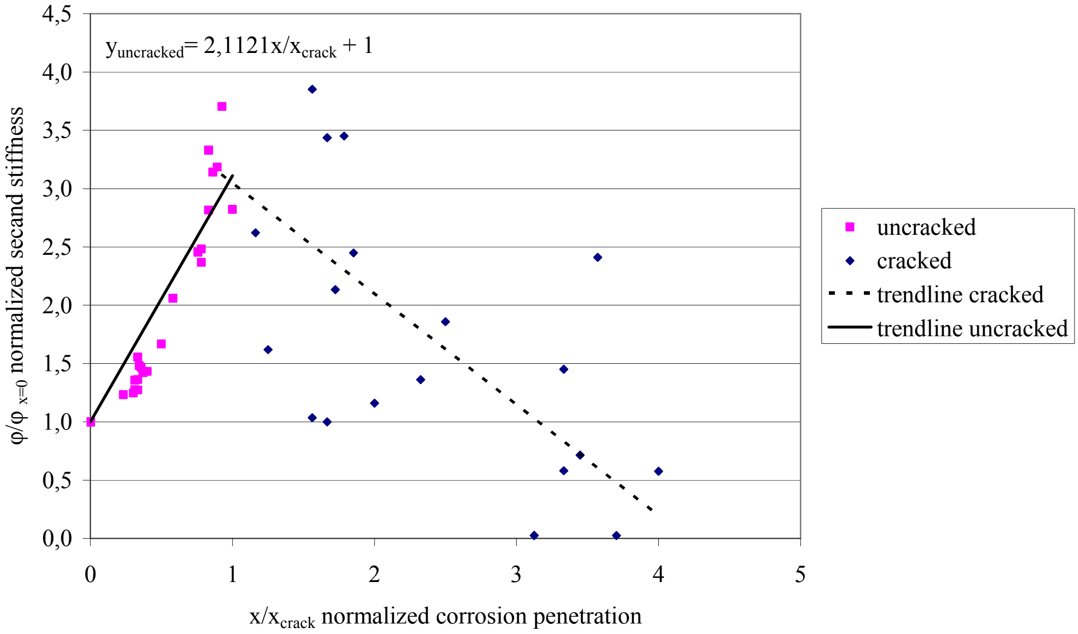

Figure 3.24 Development of the normalized secant stiffness over the normalized corrosion penetration

4 Method to Obtain the Bond-slip Response for Corroded Reinforcement

4.1 Observed pattern from the parameter study

When looking at the results of the parameter study, it became obvious that the bond-slip curves of corroded reinforcement could be estimated by the bond-slip curves of uncorroded reinforcement. This can be done by moving the bond-slip curve of the uncorroded case to the left side, see Figure 4.1. The shift to the side, Δs_x, is determined by the degree of corrosion of the curve that it should now describe. It was calculated according to equation (4.1). The same factor, *f*, as in Chapter 3.6.3 was chosen, where it was used to relate the effect of corrosion on cracking to the effect of slip on cracking. This method was applied to all bond-slip curves of the parameter study and the agreement was good, independently of the cracking mode; see Figure 4.2-4.5.

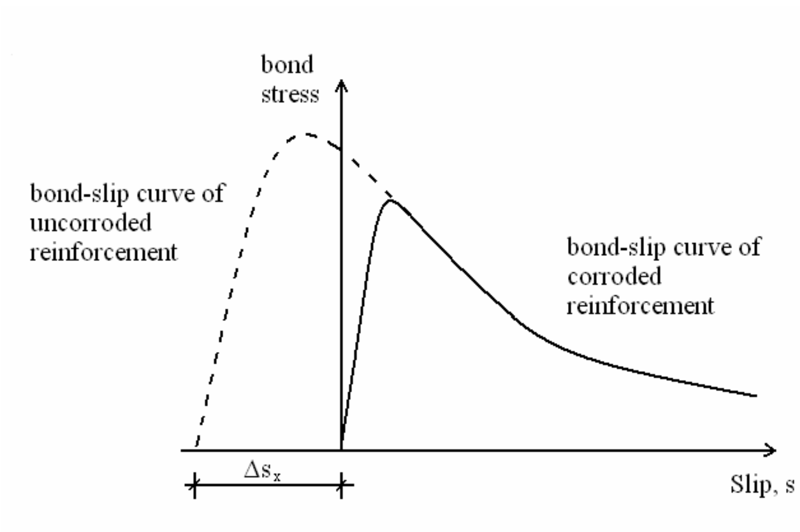

Figure 4.1 Schematic view of how to modify a bond-slip curve of uncorroded reinforcement for corroded reinforcement

When slip is applied for corroded reinforcement bond stresses develop. The stresses increase until they approximately reach the shifted bond-slip curve. Then the bond stresses tend to follow the shifted bond-slip curve; see Figure 4.2-4.5.

$$\Delta s_x = -f \cdot x \tag{4.1}$$

where

Δs_x shift to the side of the bond-slip curve for uncorroded reinforcement (in mm)

x	corrosion penetration of the corroded reinforcement (in mm)
f	factor to relate the effect of corrosion on cracking to the effect of slip on cracking, according to Chapter 3.6.3.

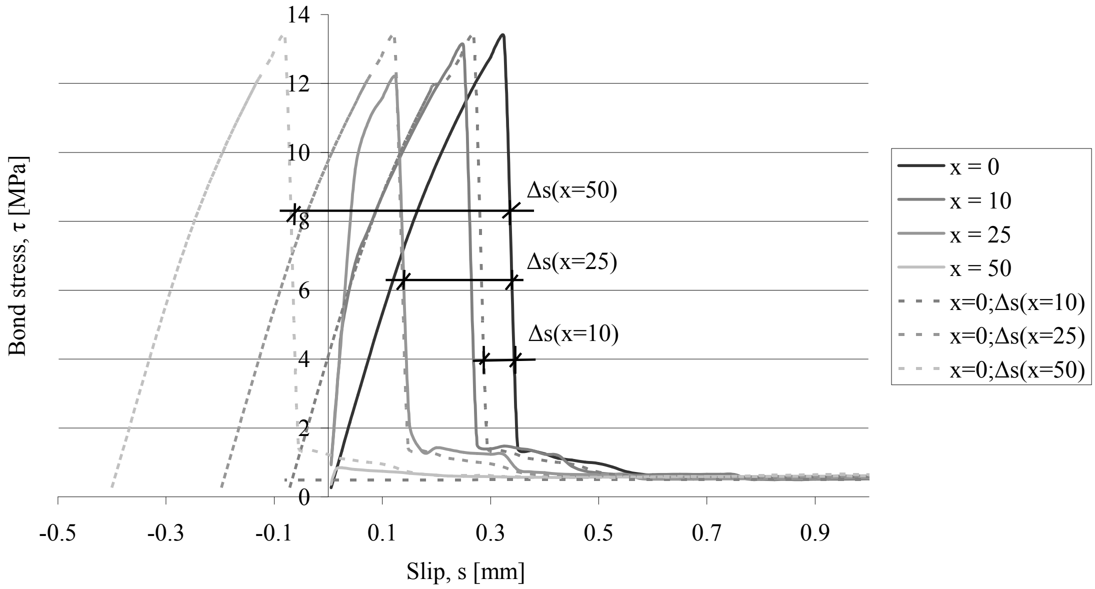

Figure 4.2 Bond-slip curves for cracking mode 1(c=45)

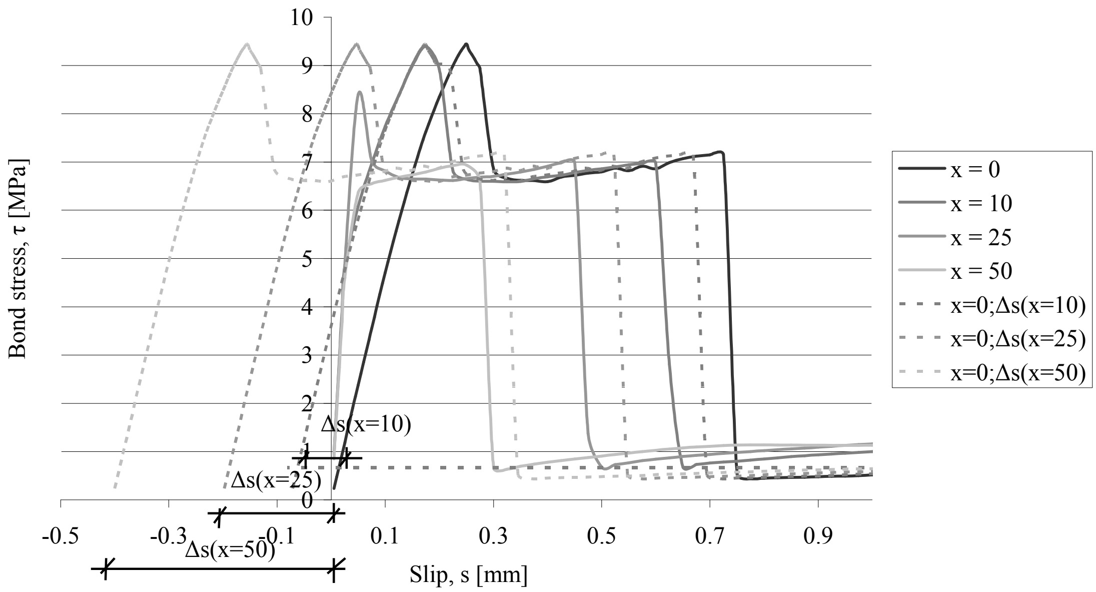

Figure 4.3 Bond-modified slip curves for cracking mode 2 (d=25)

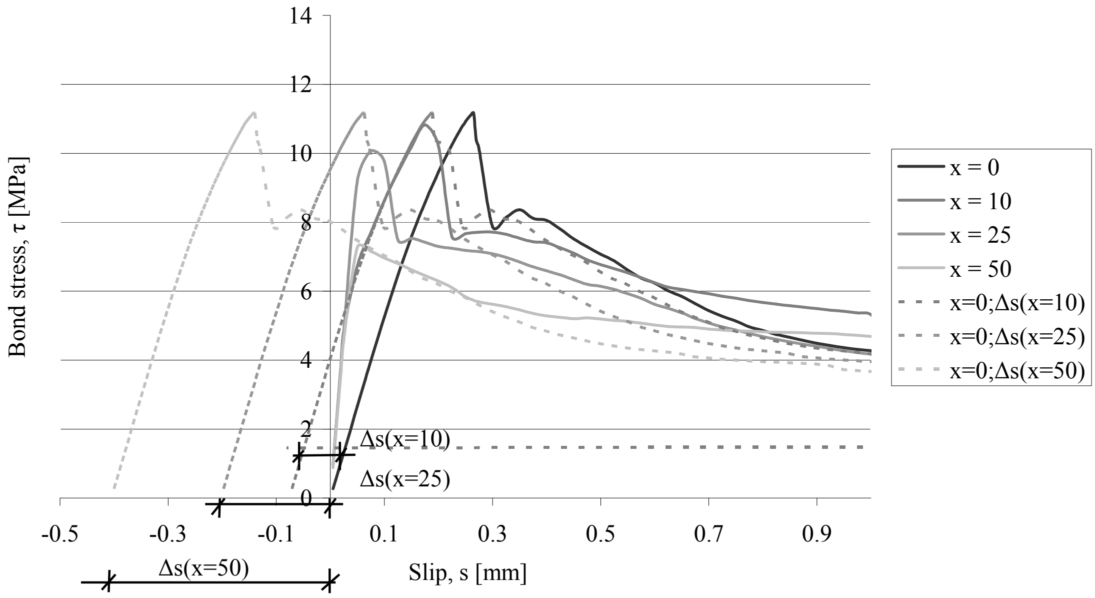

Figure 4.4 Bond-modified slip curves for cracking mode 3 (w=75)

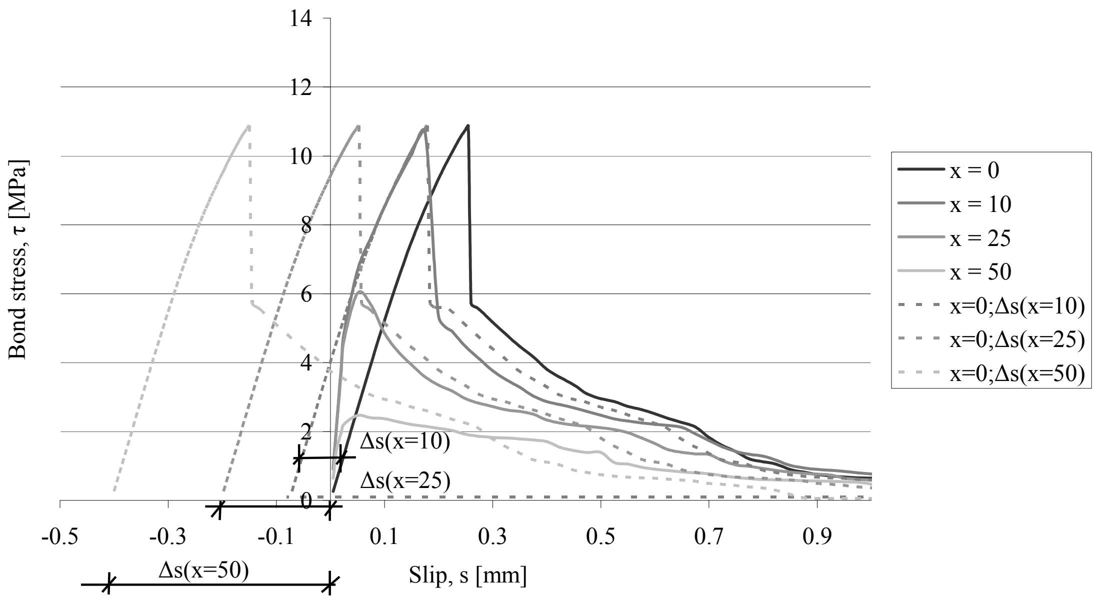

Figure 4.5 Bond-modified slip curves for cracking mode 4 (no transverse reinforcement)

4.2 Explanation of the observed pattern

As mentioned in Chapter 3, it could be observed that the development of the bond-slip response is mainly governed by the development of cracks. This is due to the fact that cracks have a high influence on the radial stresses around the reinforcement bar. These radial stresses are needed to transfer the bond stresses in the concrete.

Cracks are caused by radial deformations of the concrete around the reinforcement bars. The radial deformations that cause cracking of the cover and the crack pattern is mainly described by the geometry and the material properties. It can be assumed that the crack development and the crack pattern are independent of the source of the radial deformation. That was verified by the parameter study where the cracking modes did usually not change for applied corrosion.

As both corrosion and slip cause radial deformations, their effect could be related to each other. This was verified in Chapter 3.6.3, where the effect of corrosion on the radial deformation was added to the effect of slip on radial deformation. A modified slip was obtained that represented a radial deformation stage that could be used to predict cracking.

It can be summarized that it is possible to estimate the bond-slip response for corroded reinforcement by shifting the uncorroded bond-slip curve to the left side due to the following reasons:

- Bond stresses are related to radial stresses around the reinforcement bar.
- Every geometry has a predefined radial stress-radial deformation relationship.
- The radial deformation due to corrosion can be related to the radial deformations caused by slip.

4.3 Suggested method to obtain the bond-slip response for corroded reinforcement

The following method can be used to obtain the bond-slip response for corroded reinforcement from the bond-slip response of uncorroded reinforcement. It is valid for different loading sequences. As the bond-slip curve of uncorroded reinforcement is the base of the bond-slip curve of corroded reinforcement it is in the following called "master curve". The obtained bond-slip curve for corroded reinforcement will be called "slave curve". The terms "under the master curve" and "if the master curve is exceeded" are defined according to Figure 4.6.

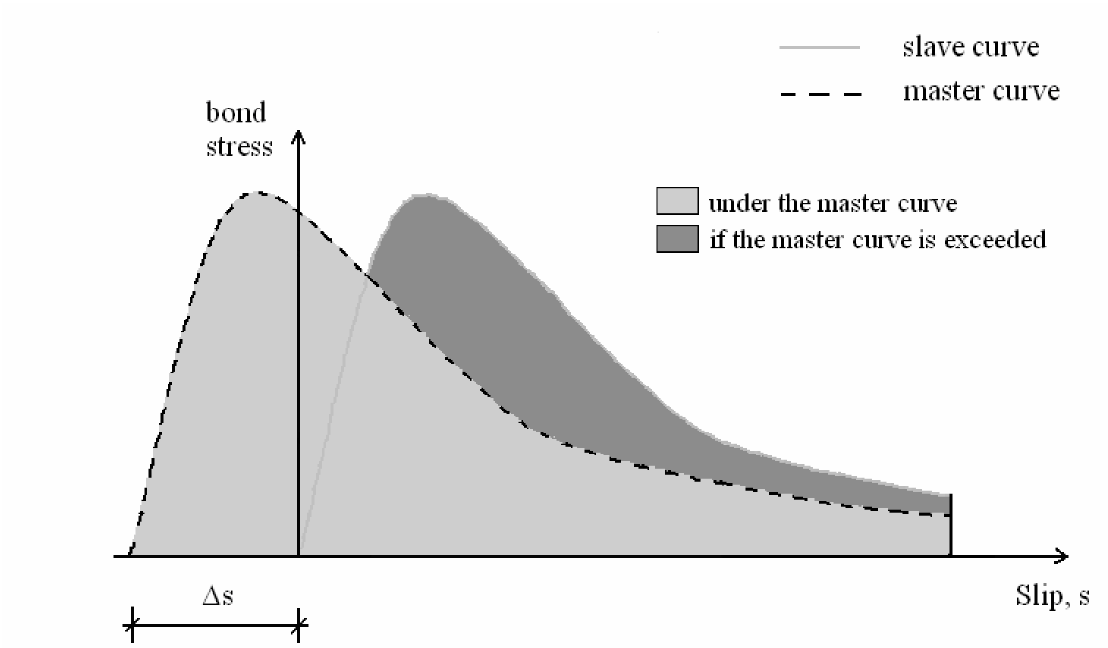

Figure 4.6 Definition of "under the master curve" and "if master curve is exceeded".

4.3.1 Scheme to obtain the slave curve from the master curve

To use the scheme, shown in Figure 4.7, it is important to distinguish between the four mentioned cases. For each case the expected stress development is described in the grey marked box. The shift of the master curve along the slip-axis is described in the last row of the scheme. After one loading has been considered it is possible to continue with the next one. In this case the instructions have to be applied on the previously obtained master and slave curve. The numbers in the boxes refer to the chapter where the boxes are explained in more detail.

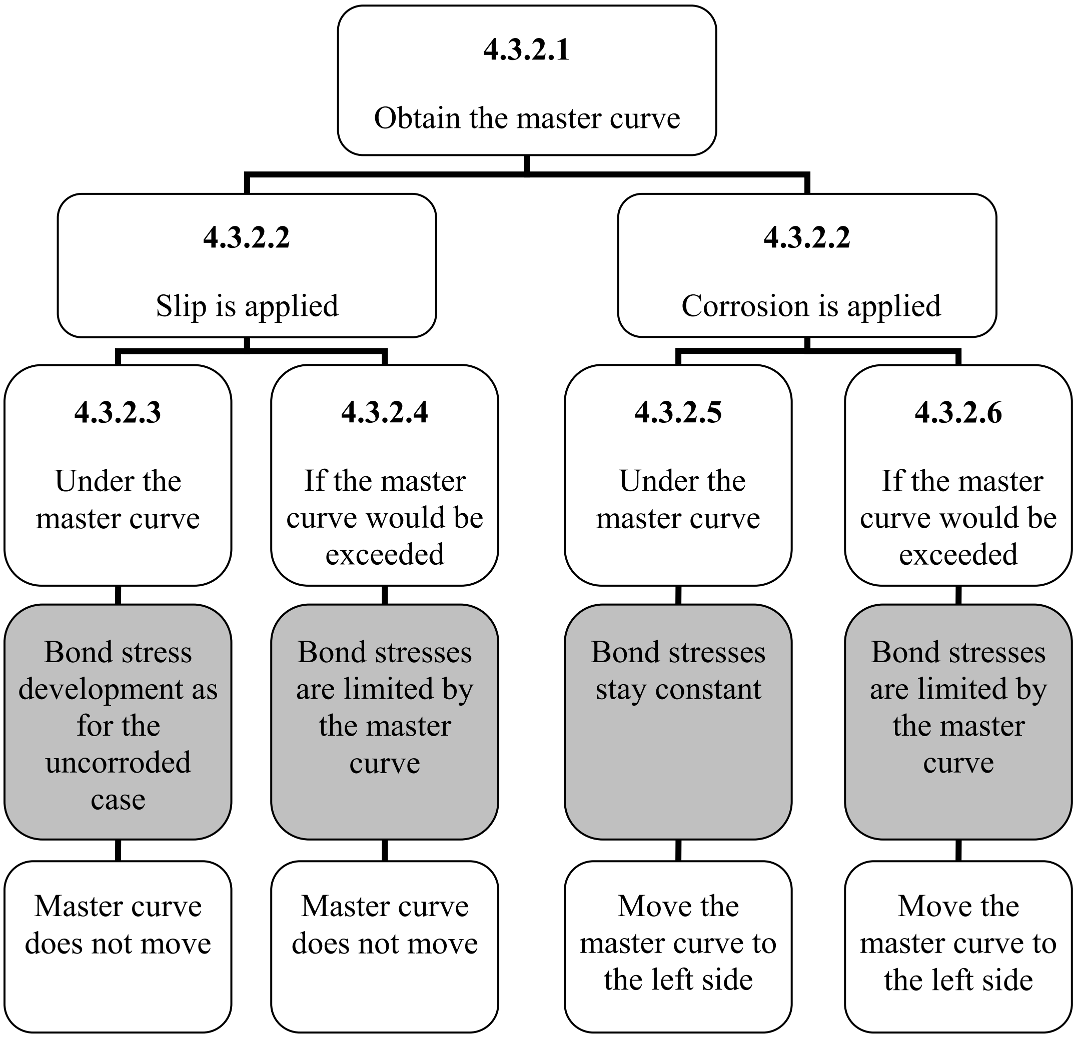

Figure 4.7 Scheme how to obtain the bond-slip response of corroded reinforcement by uncorroded reinforcement

4.3.2 Explanation of the Scheme

4.3.2.1 Obtain the master curve

In the first step the bond-slip response for uncorroded reinforcement is needed. It can be obtained by several sources such as Model Code 1990; see Chapter 5.

4.3.2.2 Distinction between applied slip and applied corrosion

Applied slip and corrosion have in common that they cause radial deformations. The difference between these cases is that applied slip causes bond stresses while applied corrosion does not show any influence on bond stresses as long as the master curve is not exceeded.

4.3.2.3 Applied slip, under the master curve

When slip is applied the bond stresses increase. For uncorroded reinforcement the slave curve and the master curve are identical. For corroded reinforcement approximately the same bond stress development as for the uncorroded case can be assumed. Therefore the first part of the master curve can be used to describe the increasing bond stresses for applied slip of the slave curve; see Figure 4.8. This is valid until the slave curve reaches the master curve.

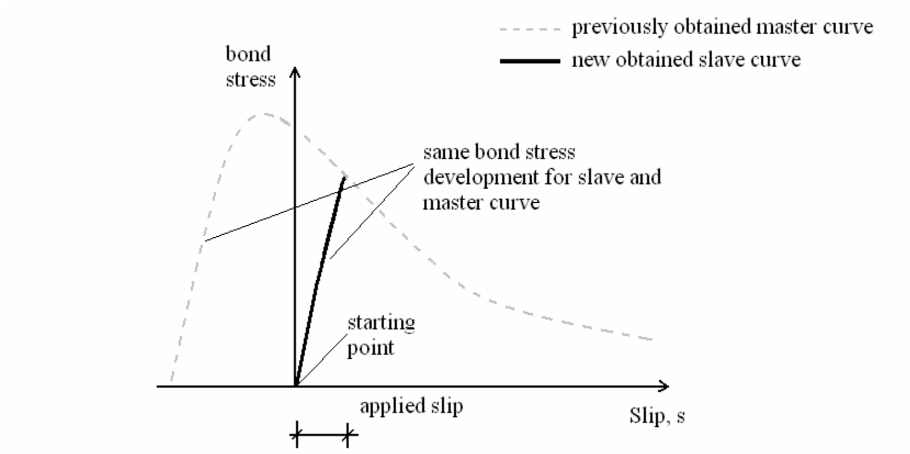

Figure 4.8 Scheme how to obtain the slave curve from the master curve for applied slip and bond stresses under the master curve

4.3.2.4 Applied slip, if the master curve would be exceeded

If for increasing slip the bond stresses of the slave curve would exceed the master curve, then the method, described in Chapter 4.3.2.3, is not valid anymore. Instead for increasing slip the bond stresses of the slave curve have to follow the master curve, see Figure 4.9. That is due to the fact, that the master curve limits the possible bond stresses for certain radial deformation stage.

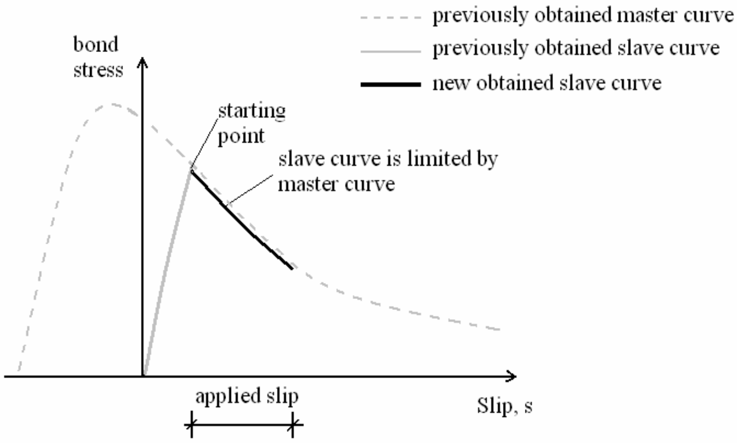

Figure 4.9 Scheme how to obtain the slave curve from the master curve for applied slip if the master curve would be exceeded

4.3.2.5 Applied corrosion, under the master curve

Corrosion does not have any effect on the bond stresses as long as the master curve is not exceeded. Therefore the bond stresses can be assumed to stay constant for applied corrosion and bond stresses under the master curve.

Corroding reinforcement causes an increase of the radial deformations. In the previous two sections the increase of these deformations was described by increasing the slip of the slave curve. This is now not possible as the corrosion has no effect on the applied slip of the slave curve. Instead the radial deformation can be considered by moving the master curve to the left side, according to equation (4.1). The shifted master curve now represents again an upper limit for the bond stresses for a certain radial deformation stage.

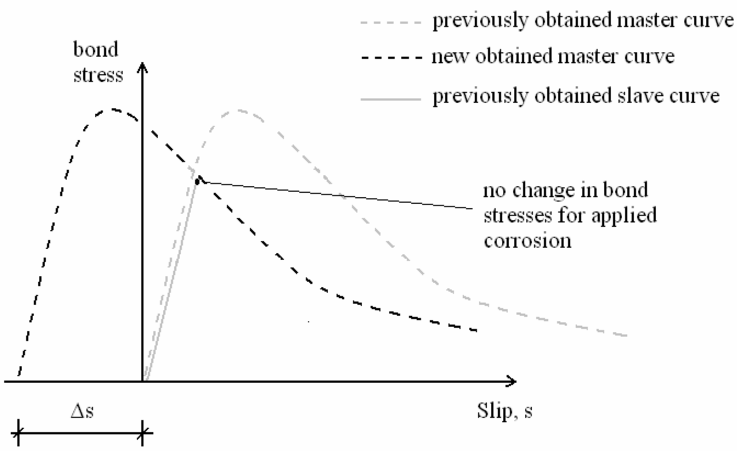

Figure 4.10 Scheme how to move the master curve for applied corrosion and bond stresses under the new obtained master curve

4.3.2.6 Applied corrosion, if the master curve would be exceeded

In this case the master curve has to be moved to the left side as described in the previous chapter.

In addition the bond stresses can not exceed the master curve. This is due to the fact that the master curve describes the maximum possible bond stresses for the new obtained radial deformation stage. Therefore the bond stresses have to drop as shown in Figure 4.11.

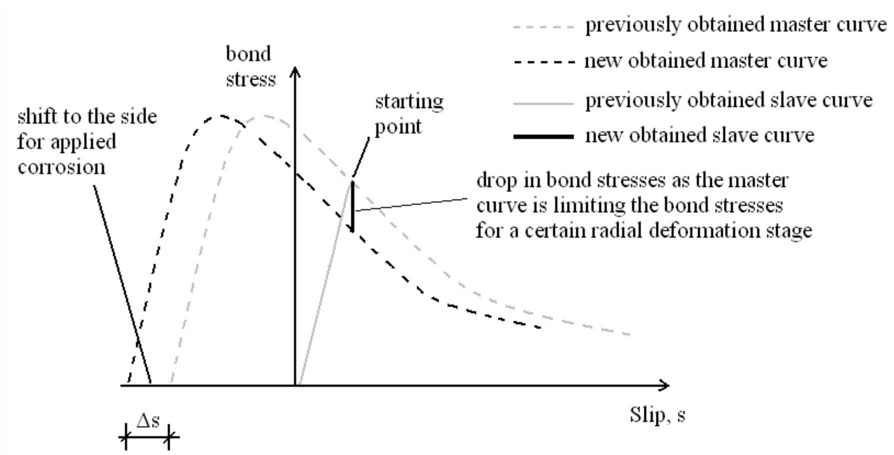

Figure 4.11 Scheme how to move the master curve for applied corrosion and how to change the bond stress if the master curve would be exceeded

4.3.3 Example

To verify that the previously described method is valid for various loading sequences an analysis was conducted with the following loading: In a first step a slip of $s_1 = 0.2$ mm was applied. Then a corrosion of $x = 25\,\mu$m was assumed. In the final step slip of $s_2 = 1.8$ mm was applied. This example is in the following used to explain and verify the method.

4.3.3.1 Obtain master curve

In the first step the master curve is needed. The master curve is the bond-slip curve for uncorroded reinforcement. In this case the master curve is obtained by the analyses for the uncorroded case; see Figure 4.12.

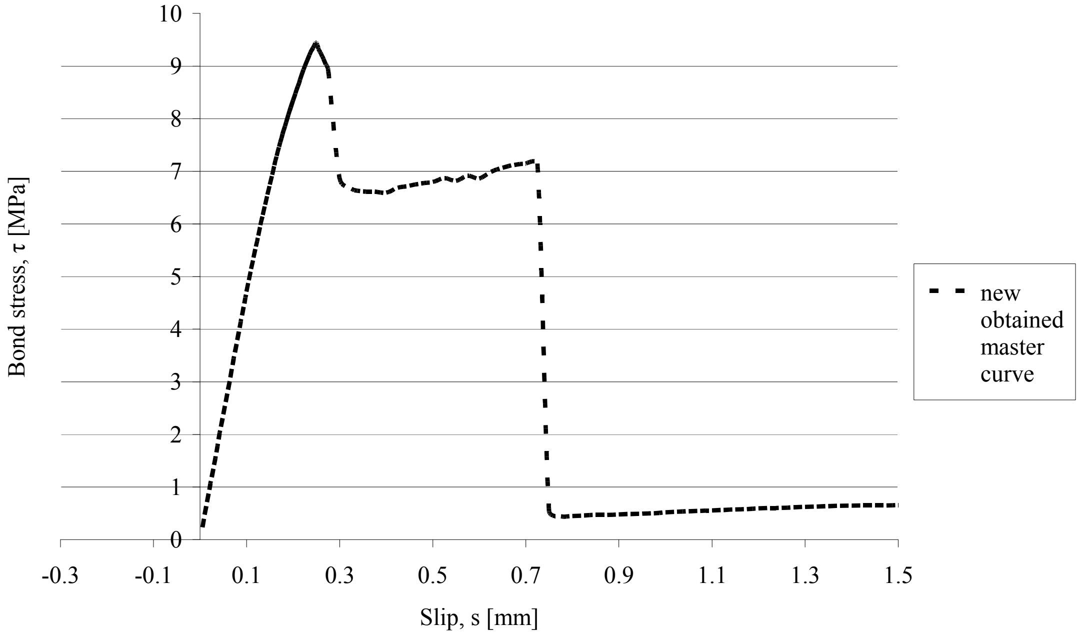

Figure 4.12 Bond-slip curve for uncorroded reinforcement

4.3.3.2 First slip is applied

For applied slip it is mentioned in Chapter 4.3.2.3 that the same bond stress development for master and slave curve can be assumed. This is valid as long as the master curve is not exceeded. For the now applied loading of $s_1 = 0.2$ mm the slave and master curves are equal, see Figure 4.13.

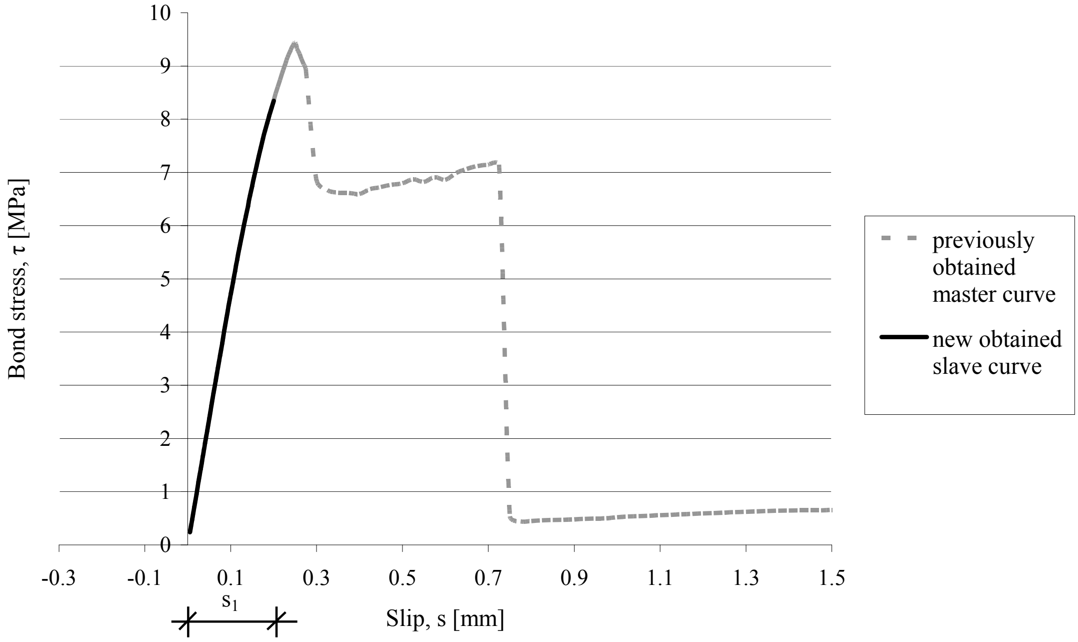

Figure 4.13 Master and slave curves after applied slip of s_1=0.2 mm

4.3.3.3 Corrosion is applied

For an applied corrosion of $x = 25\,\mu\text{m}$, it is mentioned in Chapter 4.3.2.5 and 4.3.2.6 that the master curve has to be moved to the left side according equation (4.1). In this case it leads to a shift to the side of

$$\Delta s = -8.1 \cdot 0.025 = -0.20\,\text{mm} \tag{4.2}$$

In addition it is mentioned that the bond stress stays constant for a stress state under the master curve; see Chapter 4.3.2.5. In other cases the bond stress has drop so that it does not exceed the master curve; see Chapter 4.3.2.6. This is the case here; see Figure 4.14.

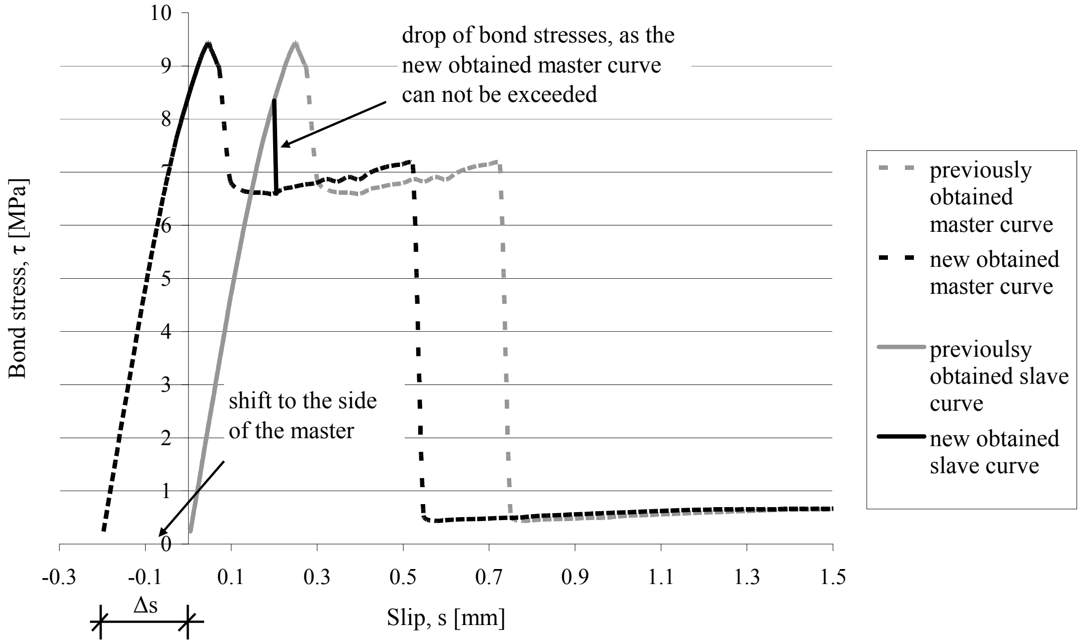

Figure 4.14 Master and slave curves after applied slip and corrosion

4.3.3.4 Second slip is applied

For applied slip the slave curve has to follow the master curve, see Chapter 4.2.3.4. Otherwise the bond stress of the slave curve would exceed the master curve; see Figure 4.15.

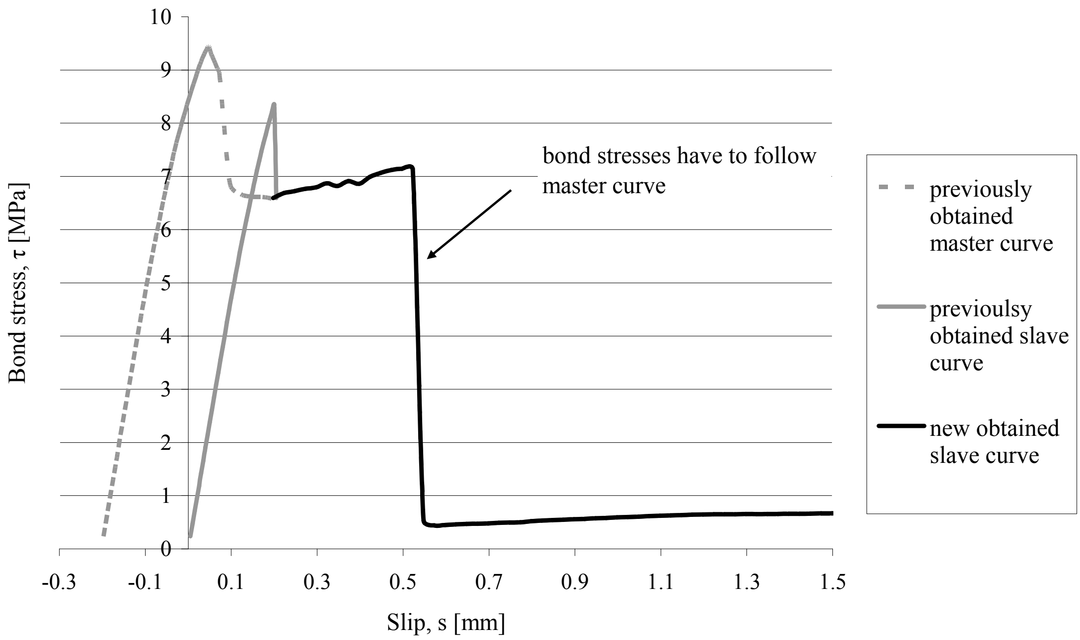

Figure 4.15 Master and slave curves after second applied slip

4.3.3.5 Final bond-slip curve

After all loading steps were considered, the final bond-slip curve is now obtained. This bond slip curve was compared with the bond-slip curve that was obtained by the FE-analysis when the mentioned loading sequence was considered; see Figure 4.16. It can be seen that the agreement is good.

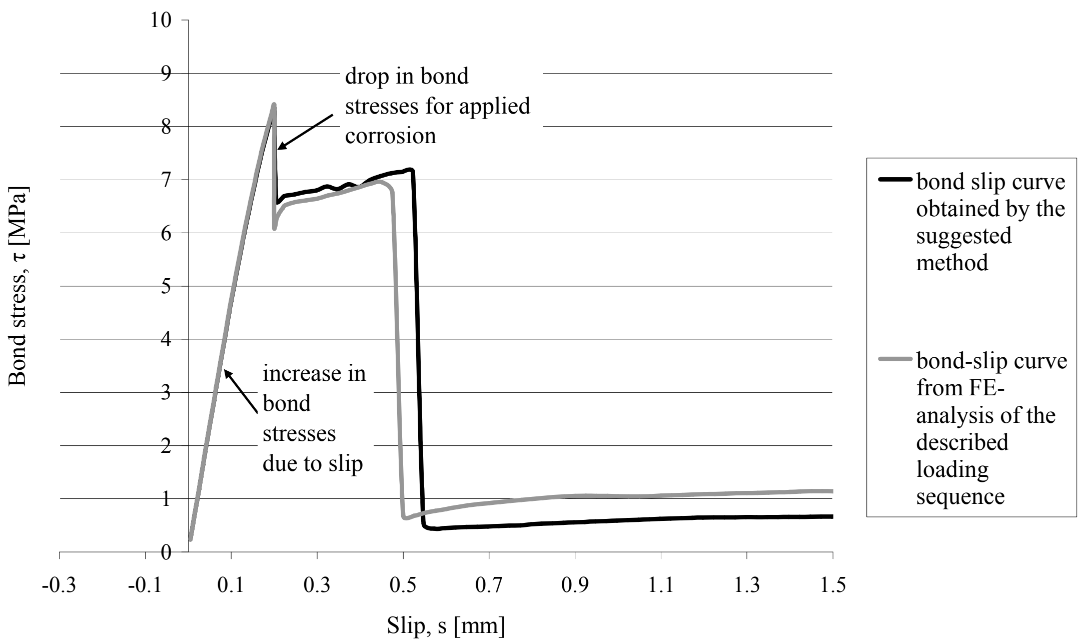

Figure 4.16 Comparison of the bond-slip curves

4.3.4 Limitations

The previously described method only holds if the assumptions mentioned in Chapter 4.2 are valid or give a good approximation of the real behaviour. Therefore, the method is only valid if the bond stress development of the uncorroded case is already governed by cover cracking; i.e. splitting failure. This only holds for smaller cover to bar diameter ratios. Different limits for this ratio are reported in the literature. In Model Code a ratio of $c_{main} / d < 5$ is proposed when no transverse pressure is applied while in CEB (2000) a ratio of $c_{main} / d < 3$ is mentioned. To be on the safe side, this method should not be used for concrete cover-to-bar diameter ratios that are larger than $c_{main} / d = 3$ when no transverse pressure is applied. For larger concrete covers or under high transverse pressure even very high applied slip can not cause a cover crack for uncorroded reinforcement. That is due to the fact that the radial deformations caused by slip have an upper limit. If the maximum radial deformations do not cause cover cracking the failure is characterised by shear failure of the concrete between the steel ribs instead of cracking of the cover. That leads to a more ductile bond-stress development than for splitting failure. As corroded reinforcement increases the radial deformations it can lead to cover cracking of specimens that would not have been cracked for uncorroded reinforcement. This can cause a sudden drop in bond stress or even lead to almost no bond stress development when the specimen is cracked before the slip applied.

The factor that relates the radial deformations caused by corrosion to the effect of slip was obtained by analysing a parameter study that was conducted by using FE-analysis. Therefore the factor has to be verified by tests before it can be trusted.

For very high amounts of reinforcement corrosion it has to be assumed that the development of a weak corrosion layer and a degradation of the rib area of the reinforcement steel have an influence on the bond properties, see Al-Sulaimani (1990). This change in the interaction between the reinforcement steel and concrete is not considered by the method. One analysed study indicated this limitation, see Chapter 6.4, while in the other studies no clue could be found to confirm this limitation.

As no reported test series could be found where the bond-slip response of corroded reinforcement for small concrete covers has been reported it was not possible to determine unerringly if the previously described hypotheses is true.

In addition the previously described method does not cover the bond stiffness increase due to corrosion.

5 Extension of the Bond-slip Model from Model Code 1990 to Corroded Reinforcement

5.1 Description of the CEB-FIP Model Code 1990

In the CEB-FIP Model Code 1990 a local bond stress-slip curve is presented for uncorroded reinforcement bars subjected to monotonic loading. For ribbed bars, the bond-slip curve consists of four different parts. The first refers to the stage where local crushing and micro-cracking occurs for small slips. The second part is a horizontal line, which appears only for well-confined concrete. In this stage crushing and shearing of the concrete between the ribs develop. The following decreasing branch represents the reduction of bond resistance due to splitting cracks along the bars. The residual bond capacity, described by a horizontal line, is maintained by transverse reinforcement which keeps a certain degree of integrity.

The Model Code distinguishes between four cases according to Table 5.1. Linear interpolation of $s_1, s_3, \tau_{\max}$ and τ_f is possible for intermediate confinement. The bond stresses can then be calculated according to equations (5.1-5.4).

$$\tau = \tau_{\max}\left(\frac{s}{s_1}\right)^{\alpha} \text{ for } 0 \le s \le s_1 \tag{5.1}$$

$$\tau = \tau_{\max} \text{ for } s_1 < s \le s_2 \tag{5.2}$$

$$\tau = \tau_{\max} - (\tau_{\max} - \tau_f)\left(\frac{s - s_2}{s_3 - s_2}\right) \text{ for } s_2 < s \le s_3 \tag{5.3}$$

$$\tau = \tau_f \text{ for } s_3 < s \tag{5.4}$$

Table 5.1 Parameters for defining the mean bond stress-slip relationship, according to CEB-FIP Model Code 1990

	Unconfined concrete		Confined concrete	
	Good bond conditions	All other bond conditions	Good bond conditions	All other bond conditions
s_1 [mm]	0.6	0.6	1.0	1.0
s_2 [mm]	0.6	0.6	3.0	3.0
s_3 [mm]	1.0	2.5	Clear rib spacing	Clear rib spacing
α	0.4	0.4	0.4	0.4
$\tau_{\max}$	$2.0\sqrt{f_{ck}}$	$1.0\sqrt{f_{ck}}$	$2.5\sqrt{f_{ck}}$	$1.25\sqrt{f_{ck}}$
τ_f	$0.15\tau_{\max}$	$0.15\tau_{\max}$	$0.40\tau_{\max}$	$0.40\tau_{\max}$

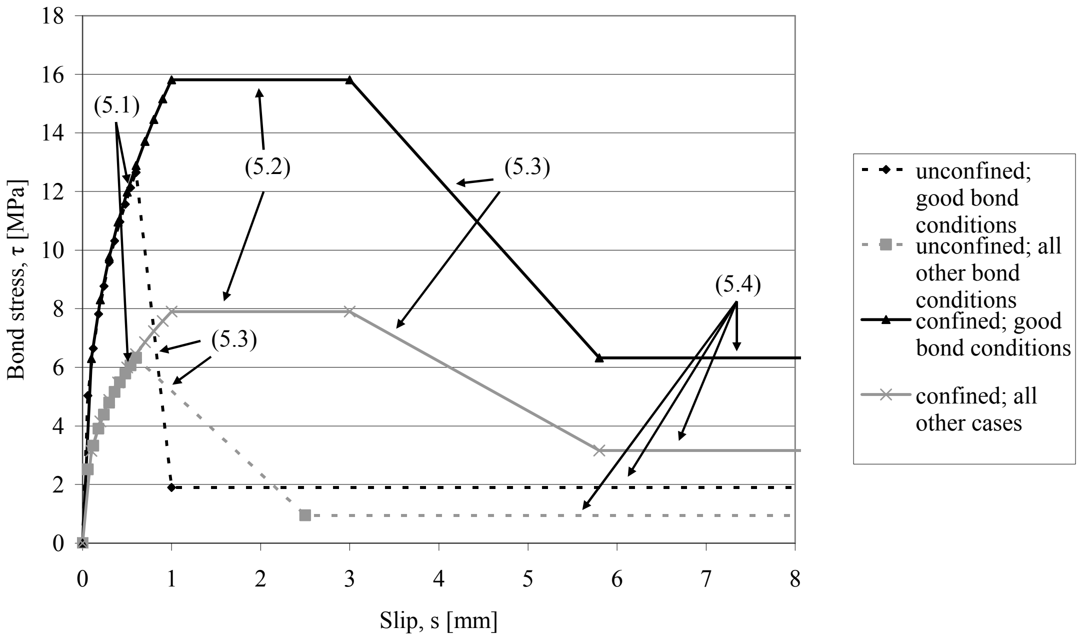

Figure 5.1 Analytical bond stress-slip relations according to CEB-FIP Model Code 1990, for concrete C40

5.2 Comparison of the uncorroded case

In the Model Code, confined conditions can be assumed when the bond failure develops by shearing of the concrete between the ribs of the reinforcement bars. Unconfined condition can be assumed when failure occurs due to splitting of the concrete. The latter applies for all specimens in the parameter study.

Special conditions are defined in the Model Code to distinguish between the confined and unconfined cases. A concrete cover $c = 1 \cdot d_{main}$ and a minimum transverse reinforcement according to equation 5.5 will lead to unconfined concrete.

$$A_{trans,\min} = 0.25 n A_s \tag{5.5}$$

where

A_{trans} area of transverse reinforcement, provided as stirrups, over a length equal to the anchorage length

n number of bars enclosed by stirrups

A_s area of one main bar

Confined concrete can be assumed for a concrete cover $c \geq 5d_{main}$, a clear bar spacing $> 10d_{main}$ or closely spaced transverse reinforcement with an area $A_{trans} > nA_s$. As can be seen in Tables 3.2 and 3.3, the analysed geometries are mainly unconfined according the Model Code. The contribution of the transverse reinforcement to the confinement is difficult to consider, as the transverse reinforcement is not provided as stirrups in the parameter study. In addition the Model Code defines the transverse reinforcement, A_{trans}, as the area of transverse reinforcement over a length equal to the anchorage length without defining the anchorage length. It still can be assumed that the amount of transverse reinforcement in the parameter study is far away from providing confinement.

Table 5.2 Comparison of concrete covers

Concrete cover				
Model Code 1990		parameter study		
unconfined	confined	mean geometry	min.	max.
$>1d_{main}$	$>5d_{main}$	$1.5d_{main}$	$1.2d_{main}$	$3d_{main}$

Table 5.3 Comparison of clear spacing

Clear spacing				
Model Code 1990		parameter study		
unconfined	confined	mean geometry	min.	max.
-	$>10d_{main}$	$4d_{main}$	$3d_{main}$	$14d_{main}$

Usually good bond-conditions can be assumed for bond tests. The specimens are mainly small, well compacted and the reinforcement bars are most often not placed at the top of the specimens. As the bond model, described in Chapter 2.1, has been adjusted to this kind of tests it can be expected to fit best with good bond conditions.

Therefore, it is seems natural to compare the results from the parameter study mainly with good bond conditions in unconfined concrete according to the Model Code. In Figure 5.2 and Figure 5.3 the bond-slip curves of the Model Code are shown together with the bond-slip curves of the parameter study. Only uncorroded cases for a concrete type C40 are compared.

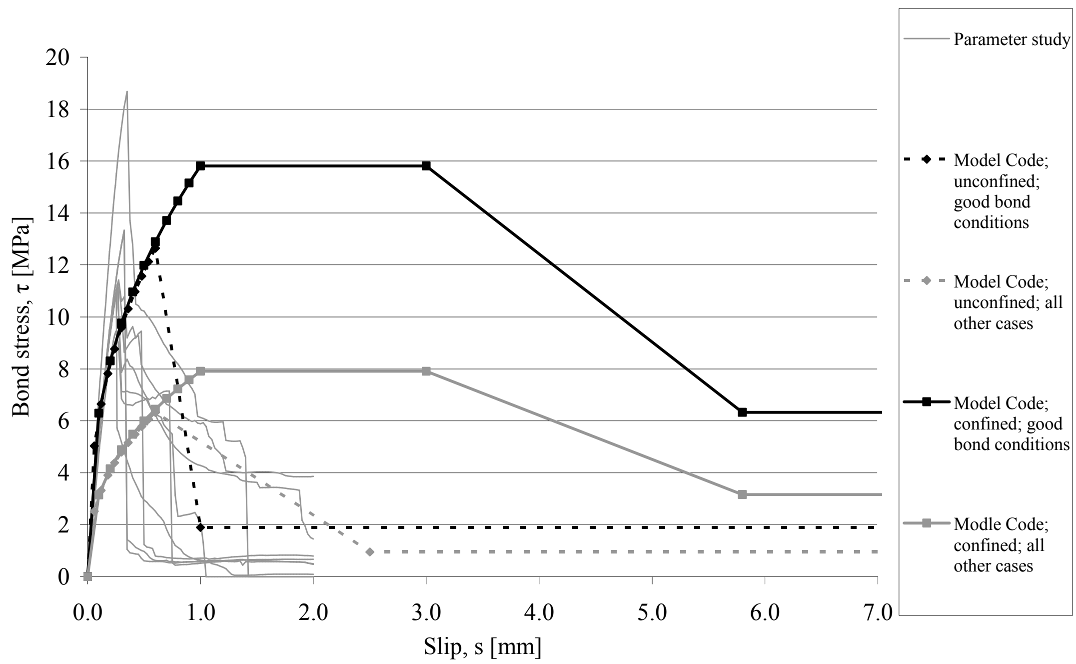

Figure 5.2 Comparison of bond-slip curves of the parameter study and the CEB-FIP Model Code 1990 for concrete C40

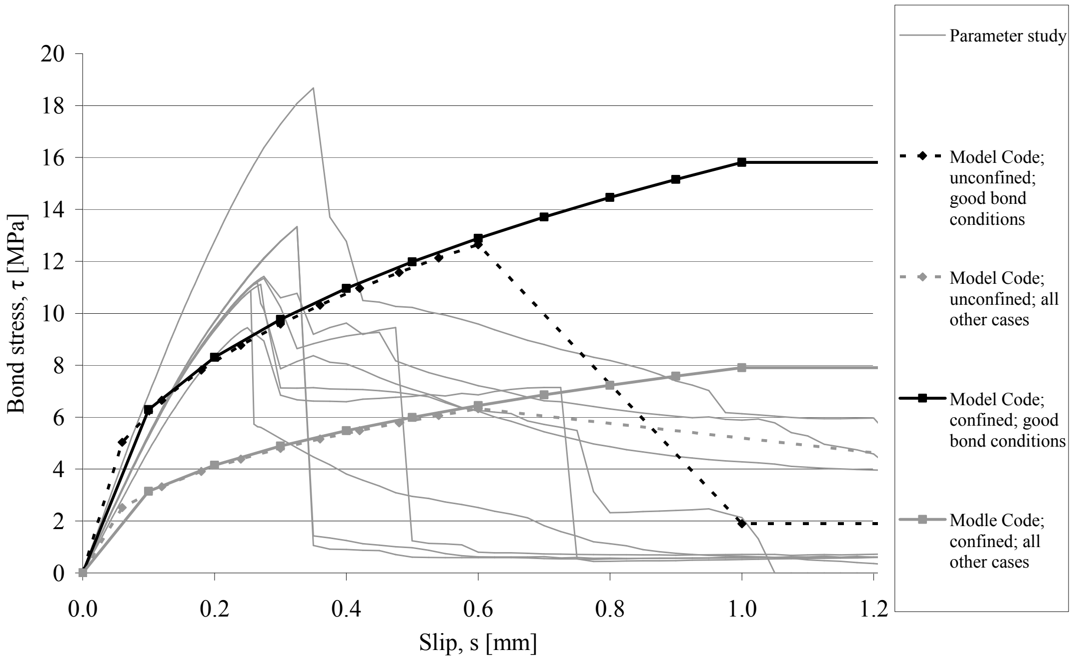

Figure 5.3 Comparison of bond-slip curves of the parameter study and the CEB-FIP Model Code 1990 for concrete C40 (detail of Figure 5.2)

As expected, the results agree best with the unconfined concrete with good bond conditions. In Table 5.4 the mean bond strengths of unconfined concrete with good bond conditions according to Model Code is compared with the mean bond strength obtained from the parameter study. Good agreement is obtained for all concrete types.

Table 5.4 Comparison of bond strength

Concrete type	Bond strength according to Model Code 1990, unconfined, good bond conditions [MPa]	Mean bond strength of the parameter study [MPa]	Relative error
C20	8.94	7.43	-16.9%
C40	12.65	11.72	-7.4%
C80	17.89	17.28	-3.4%

5.3 Modification of the Model Code 1990

The here described method is valid for reinforcement that is corroded before the pull-out is applied. For other loading sequences see Chapter 4.3. Now an additional parameter is needed as input to predict the bond-slip response. The corrosion penetration, x, is needed to calculate the shift of the bond-slip curve of the uncorroded case. This is done according to the following equation:

$$\Delta s = -8.1 \cdot x \tag{5.6}$$

where

Δs is the shift of the bond-slip curve of uncorroded reinforcement along the x-axis (in mm)

x is the corrosion penetration (in mm)

The shift along the x-axis is considered in Table 5.5 and in equations (5.8-5.10). The shifted bond-slip curve for uncorroded reinforcement is used as an upper limit of the bond stresses. As soon as the bond stresses reach this upper limit they have to follow the shifted curve for further applied slip.

The bond stress development for corroded reinforcement can be approximated by the bond stress development for uncorroded reinforcement as long as the shifted bond-slip curve is not exceeded. The following equations are needed to obtain the bond-slip response:

$$\tau = \tau_{\max}\left(\frac{s}{s_1}\right)^{\alpha} \text{ for } 0 \le s \le s_1 \tag{5.7}$$

$$\tau = \tau_{\max} \text{ for } s_{1shifted} < s \le s_{2shifted} \tag{5.8}$$

$$\tau = \tau_{\max} - (\tau_{\max} - \tau_f)\left(\frac{s - s_{2shifted}}{s_{3shifted} - s_{2shifted}}\right) \text{ for } s_{2shifted} < s \le s_{3shifted} \tag{5.9}$$

$$\tau = \tau_f \text{ for } s_{3shifted} < s \tag{5.10}$$

Table 5.5 Parameters for defining the mean bond stress-slip relationship, according to CEB-FIP Model Code 1990

	Unconfined concrete		Confined concrete	
	Good bond conditions	All other bond conditions	Good bond conditions	All other bond conditions
$s_{1shifted}$ [mm]	$0.6+\Delta s$	$0.6+\Delta s$	$1.0+\Delta s$	$1.0+\Delta s$
$s_{2shifted}$ [mm]	$0.6+\Delta s$	$0.6+\Delta s$	$3.0+\Delta s$	$3.0+\Delta s$
$s_{3shifted}$ [mm]	$1.0+\Delta s$	$2.5+\Delta s$	Clear rib spacing $+\Delta s$	Clear rib spacing $+\Delta s$
s_1 [mm]	0.6	0.6	1.0	1.0
α	0.4	0.4	0.4	0.4
$\tau_{\max}$	$2.0\sqrt{f_{ck}}$	$1.0\sqrt{f_{ck}}$	$2.5\sqrt{f_{ck}}$	$1.25\sqrt{f_{ck}}$
τ_f	$0.15\,\tau_{\max}$	$0.15\,\tau_{\max}$	$0.40\,\tau_{\max}$	$0.40\,\tau_{\max}$

Then three different cases have to be considered:

- For $0 \le s_1 \le s_{2shifted}$ the bond-slip response has to be calculated according to

  equation (5.7) for $0 \le s \le s_1$

  equation (5.8) for $s_1 < s \le s_{2shifted}$

  equation (5.9) for $s_{2shifted} < s \le s_{3shifted}$

  equation (5.10) for $s_{3shifted} < s$; see Figure 5.4.

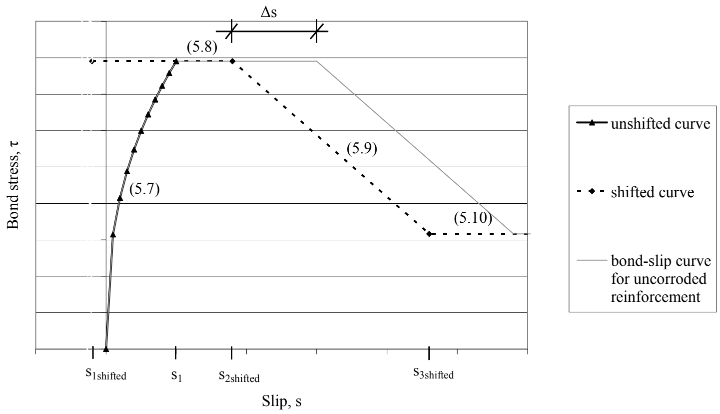

Figure 5.4 Bond-slip curve for $0 \le s_1 \le s_{2shifted}$

- For $s_{2shifted} < s_1 \le s_{3shifted}$ the bond-slip response has to be calculated according to

$$\min\begin{Bmatrix} equation(5.7) \\ equation(5.9) \end{Bmatrix} \text{ for } 0 \le s \le s_{3shifted}$$

equation (5.10) for $s_{3shifted} < s$; see Figure 5.5.

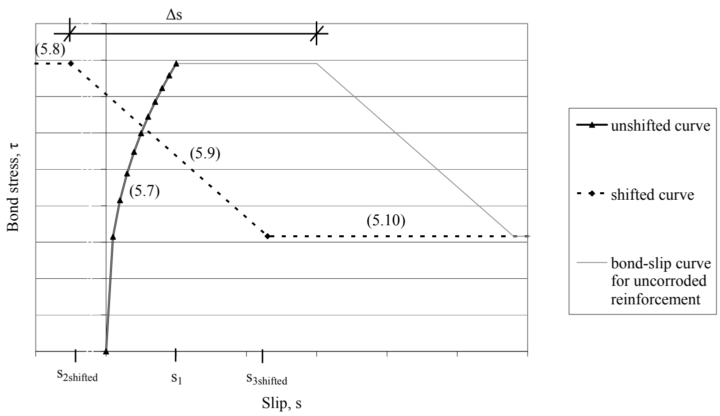

Figure 5.5 Bond-slip curve for $s_{2shifted} < s_1 \le s_{3shifted}$

- For $s_{3shifted} < s_1$ the bond-slip response has to be calculated according to

$$\min\begin{Bmatrix} equation(5.7) \\ equation(5.10) \end{Bmatrix}; \text{ see Figure 5.6.}$$

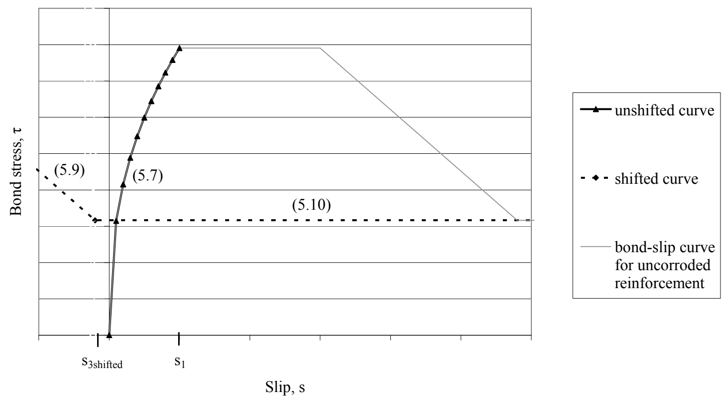

Figure 5.6 *Bond-slip curve for* $s_{3shifted} < s_1$

5.3.1 Limitations

Besides the limitations mentioned in Chapter 4.3.4 it has to be considered that the reliability of the bond model described in Model Code has to be further assessed before it can be used directly in real applications. The same holds for the modified bond model described in Chapter 5.3.

6 Comparison of the Results

The bond strength obtained by the modified Model Code was compared with two different reported test series; see Chapter 6.1 and 6.2. Another test series was analysed that showed a change in failure mode; see Chapter 6.3. Finally, a test series was used to check if it is possible to relate the effect of corrosion on failure to the effect of slip; see Chapter 6.4.

6.1 Bond strength of corroded bars according to Rodriguez (1994)

6.1.1 Description of the tests and results

Rodriguez tested cubic concrete specimens with four bars in the corners, with and without stirrups, see Figure 6.1. The main parameters that were varied were level of corrosion, cover-to-bar diameter ratio, the bar position and the amount of stirrups, see Table 6.1. Only the main reinforcement bars were corroded by applying a current.

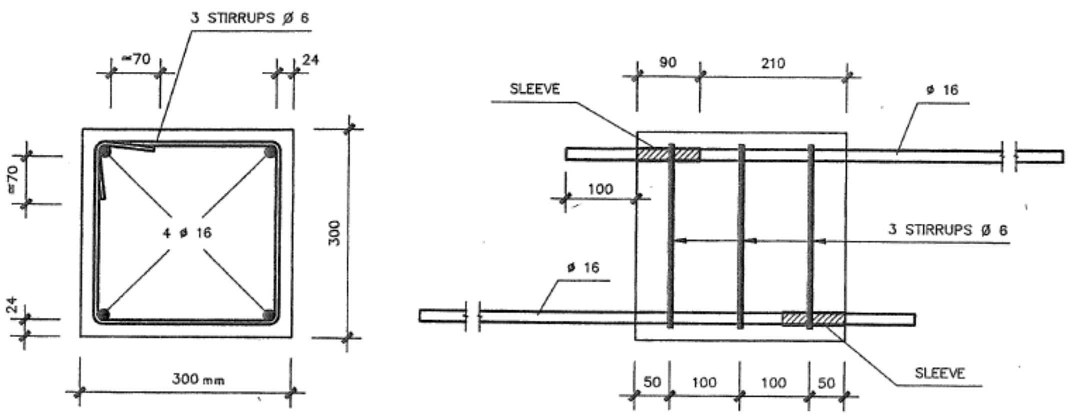

Figure 6.1 Type 2 specimens for bond test according to Rodriguez (1994).

Table 6.1 Specimens for bond tests according to Rodriguez (1994).

Specimens type	Main bar diameter d_{main} [mm]	Stirrups diameter d_{trans} [mm]	Stirrups spacing s [cm]	Concrete cover c_{main} [mm]
1	16	8	7	24
2	16	6	10	24
3	16	-	-	24
4	16	6	10	40
5	10	6	10	15

For uncorroded bars almost no influence of the amount of stirrups on bond strength has been observed. In contrast stirrups had a significant influence when specimens with corroded bars were tested. The bond strength of highly corroded bars without stirrups was close to zero while the presence of stirrups resulted in a residual strength of 3.0-4.0 N/mm^2. For specimens with a cracked cover due to reinforcement corrosion the influence of c/d_{main} was negligible. A regression analysis has been carried out and led to the following expression:

$$\tau_{\max} = K \cdot x^{-K'} \tag{6.1}$$

where

$\tau_{\max}$ is the bond strength in N/mm^2

x is the corrosion penetration in μm

K, K' are constants to fit with experimental results, see Table (2.4)

The bond strength versus decrease of rebar radius is shown in Figure 6.2.

Table 6.2 Values of fitting constants according to Rodriguez (1994).

Type of specimen	K		K'	
	Top reinforcement	Bottom reinforcement	Top reinforcement	Bottom reinforcement
1	7.03	7.43	0.067	0.098
2	5.05	5.83	0.035	0.051
3	4.11	4.17	0.153	0.194
4	6.55	6.98	0.066	0.088
5	5.38	5.53	0.021	0.043

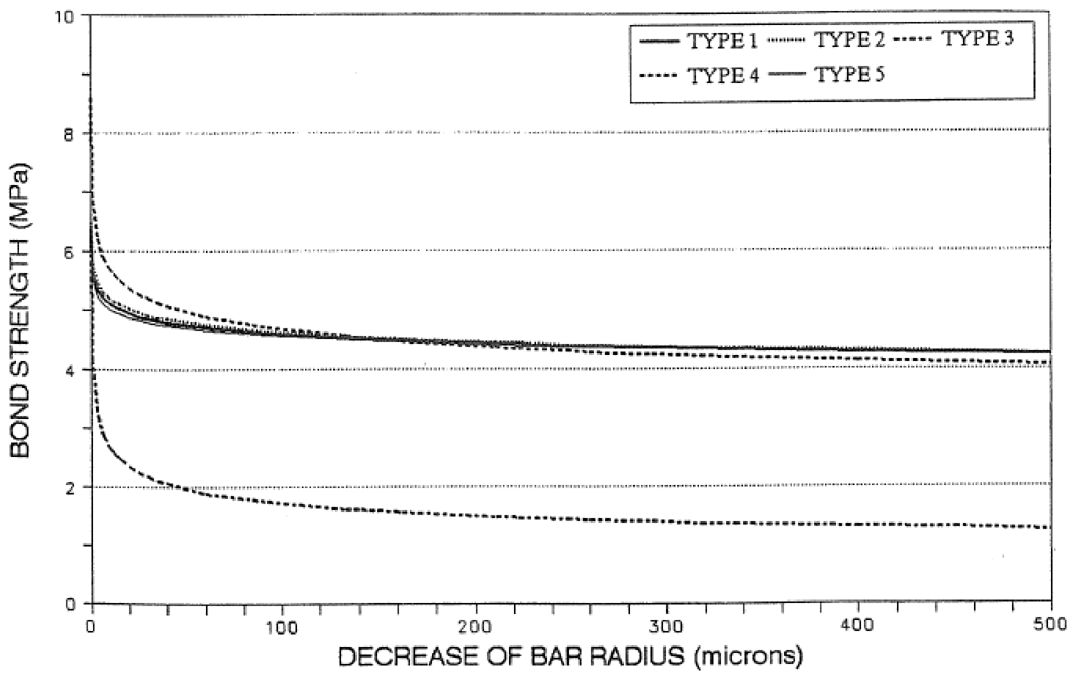

Figure 6.2 Bond strength versus decrease of rebar radius for bottom cast bars according to Rodriguez (1994)

6.1.2 Comparison to the modified Model Code

In the Model Code it is not clearly defined how to obtain the bond-slip response for intermediate confinements. Therefore it was chosen to study type 2 specimens according to Rodriguez (1994), that agreed quite well with the unconfined case according to Model Code, see Table 6.3.

Table 6.3 Evaluation of the degree of confinement for type 2 specimens

	Type 2 specimen	Unconfined according to Model Code	Confined according to Model Code
concrete cover c	$1.5 \cdot d_{main}$	$1.0 \cdot d_{main}$	$5.0 \cdot d_{main}$
transverse reinforcement A_{st} [mm^2]	$A_{st} = 3/2 \cdot \pi \cdot 3^2$ $= 42.4$	$A_{st,\min} = 0.25 \cdot n \cdot A_s$ $= 50.3$	$A_{st,\min} \geq n \cdot A_s$ $= 201.1$

The method described in Chapter 5.3 was applied for different corrosion penetrations. The bond-slip curve from the modified Model Code for unconfined concrete was used and the bond strength was reported. Good bond conditions were assumed. The obtained bond strength development over the corrosion penetration is shown in Figure 6.3 and compared with the reported test results.

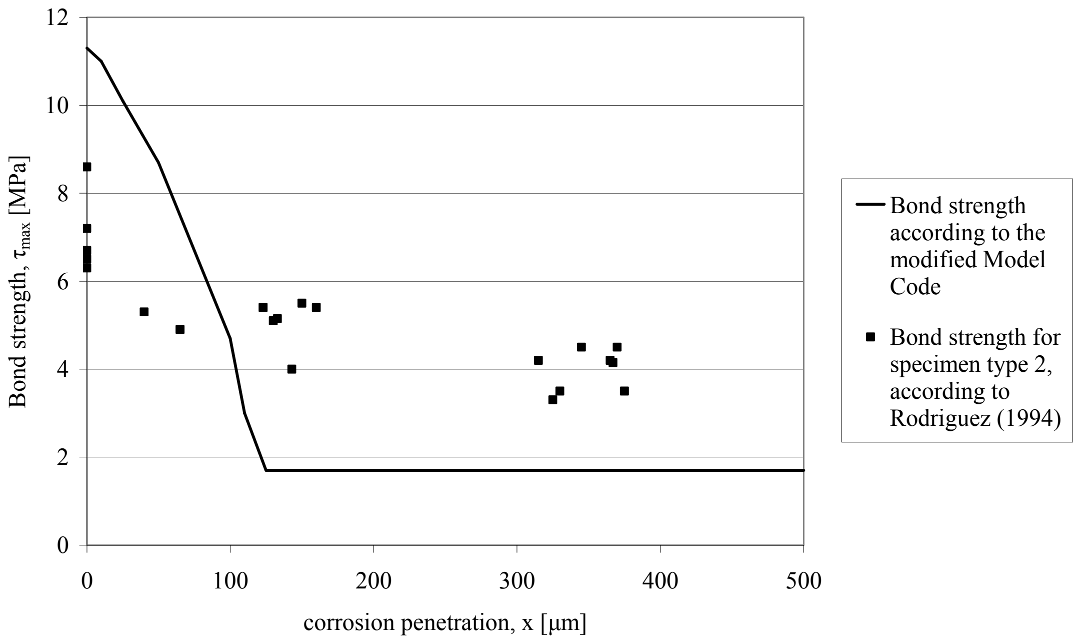

Figure 6.3 Comparison of the bond strength versus corrosion penetration for specimen type 2, according to Rodriguez (1994) and the modified Model Code

It can be seen that already for the uncorroded reinforcement the difference in bond strength is high. For the performed tests an average bond strength of $\tau_{\max} = 6.5$ MPa has been reported for bottom cast reinforcement. By applying the Model Code a bond strength of $\tau_{\max} = 11.3$ MPa was obtained.

In addition the decrease of the bond stress is overestimated by the modified Model Code. That could be due to the fact, that corner bars have been tested. The confinement of corner bars due to stirrups was not considered in the modification of the Model Code.

6.2 Bond strength of corroded reinforcement bars according to Shima (2002)

6.2.1 Description of the tests

Shima tested concrete prisms in which one steel bar was eccentrically embedded, see Figure 6.4. The effect of different concrete covers, degrees of corrosion and amounts of transverse reinforcement on bond strength were studied. The specimens were soaked in an artificial salt solution and the corrosion was accelerated by an applied current. After that a pull-out force was applied by an oil jack.

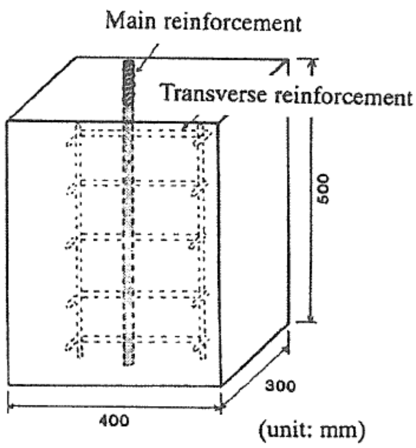

Figure 6.4 Test specimen, according to Shima (2002)

6.2.2 Comparison to the modified Model Code

The modified Model Code was used to predict the bond strength development over the degree of corrosion. The test series with a concrete cover of $c_{main}=25$ *mm* and a cover-to-bar ratio of $c_{main} / d = 1.12$ was compared with the modified Model Code for unconfined concrete and good bond conditions. The normalized bond strength was plotted over the weight loss of the reinforcement bar, see Figure 6.5.

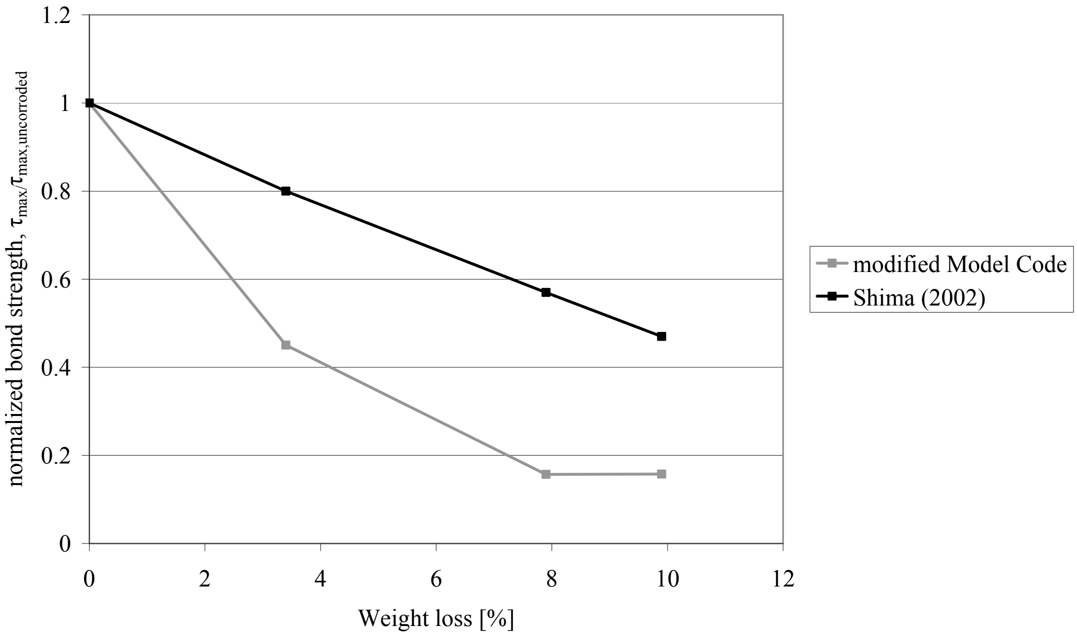

Figure 6.5 Development of the bond strength over the degree of corrosion for test according to Shima (2002) and the modified Model Code

It can be seen that the modified Model Code overestimates the decrease of the bond strength for applied corrosion.

6.3 Effect of reinforcement corrosion on bond strength according to Almusallam (1995)

6.3.1 Description of the performed tests and results

Cantilever bond test specimens have been used to study the effect of corrosion on bond, see Figure 6.6. Current has been used to accelerate the reinforcement corrosion. The degree of corrosion has been measured according to the weight loss method. The appearance of the first crack was monitored. The load-slip response has been reported, see Figure 6.7. A change in failure mode from pull-out failure for specimens with corrosion penetrations up to $x = 123$ µm to splitting failure for higher corrosion penetrations has been reported.

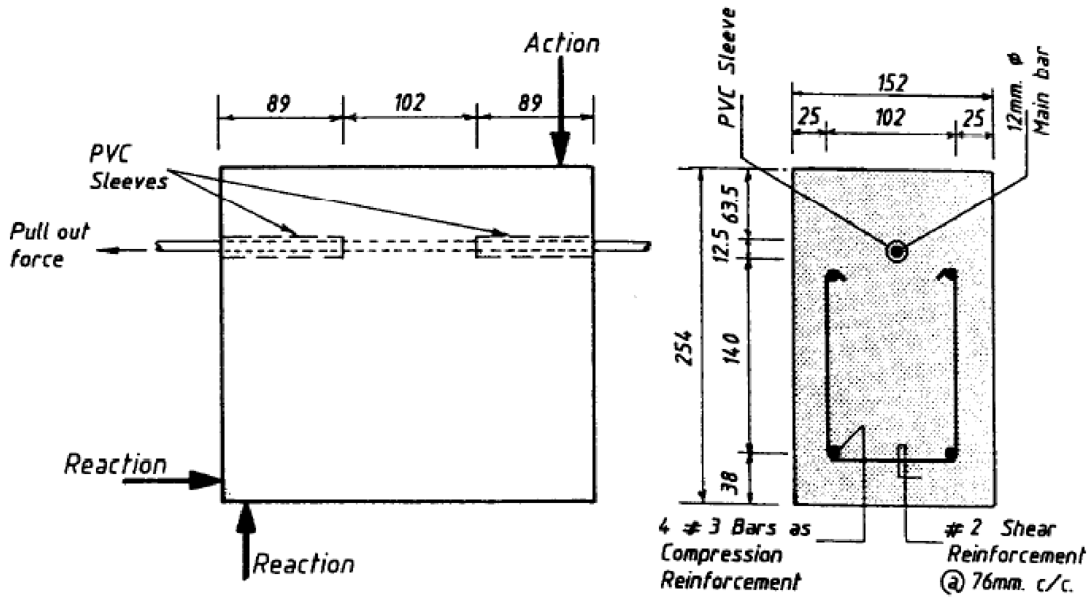

Figure 6.6 Design details of the cantilever bond test specimens, according to Almusallam (1995)

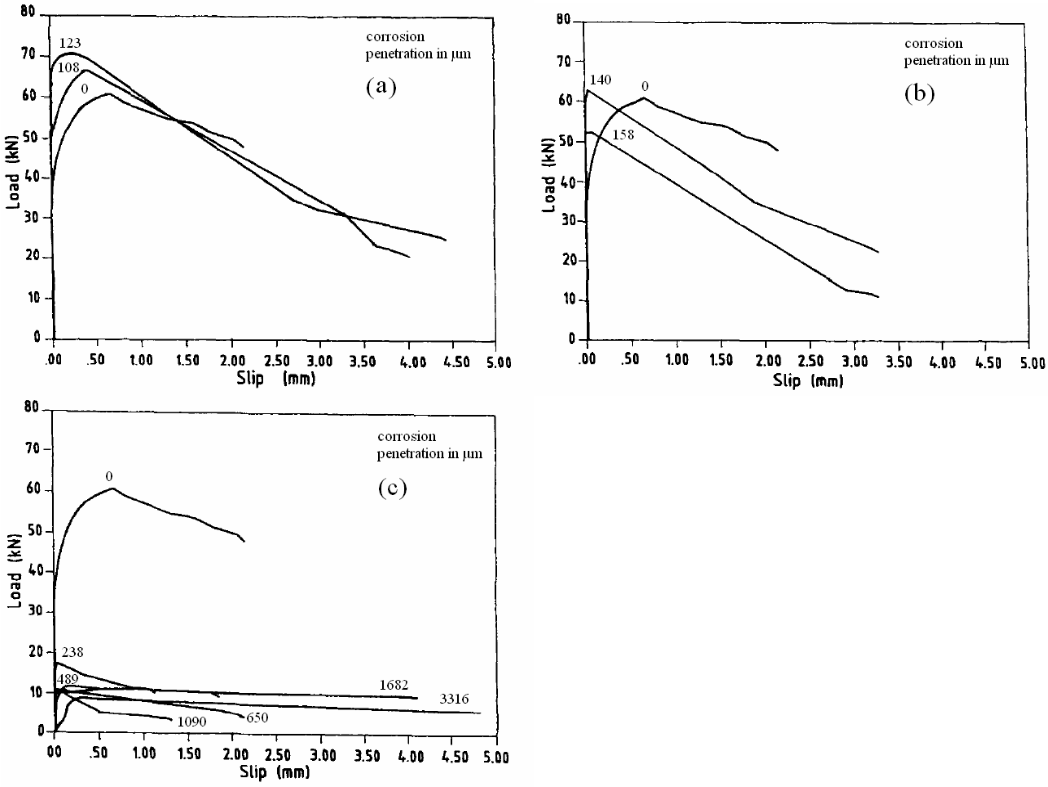

Figure 6.7 Relationship between load and slip in (a) the pre-cracking stage, (b) the cracking stage and (c) the post-cracking stage, modified from Almusallam (1995)

6.3.2 Comparison to the method with modified slip

It was difficult to predict the bond-slip response by using the Model Code. A high cover to bar diameter ratio of $c_{main} / d = 5{,}83$ provided confinement, while no transverse reinforcement had been used to keep a certain degree of integrity after cracking.

For this high cover to bar ratio, the failure mode changed when a corrosion penetration of $x = 238$ µm had been applied. The drastic change in the bond strength and the dissipated energy due to corrosion becomes obvious when comparing the bond-slip curves for $x = 158$ µm and $x = 238$ µm. The failure mode change can not be predicted by the modified Model Code. Therefore it has been chosen to limit the area of validity of the modified Model Code to concrete cover-to-bar diameters ratios that are smaller than three.

In Figure 6.8 the bond-slip curve for corroded reinforcement are shifted in the negative direction according to equation (4.1). This should lead to congruent force-slip curves. It can be seen that the agreement is feasible as long as the failure mode did not change.

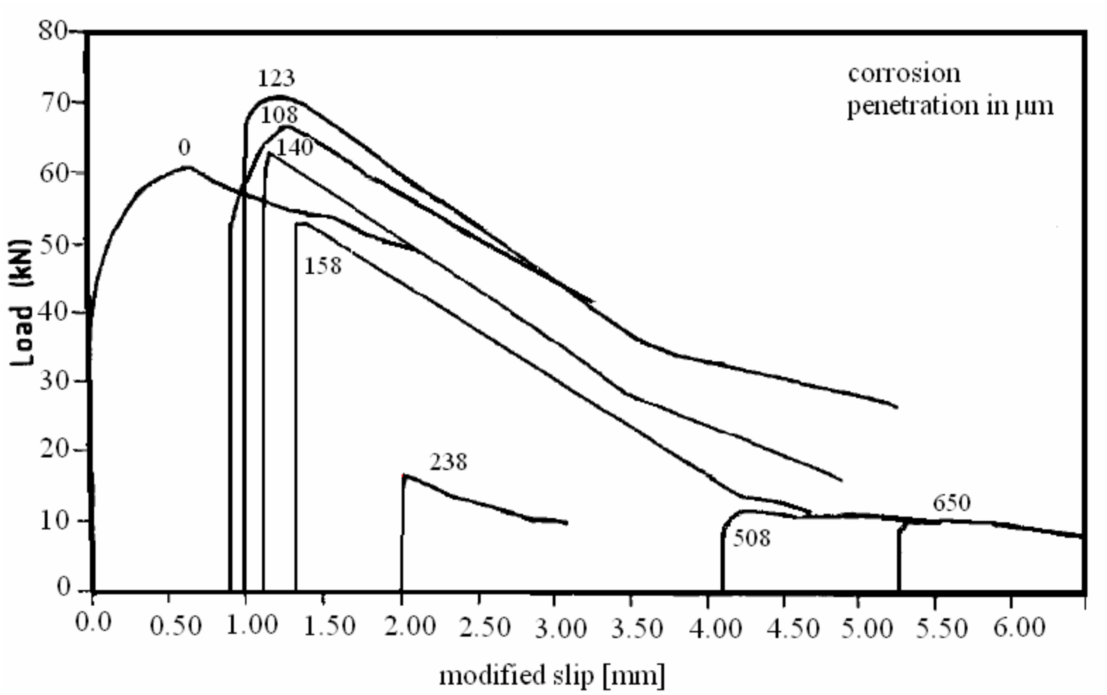

Figure 6.8 Force-modified slip curves for different corrosion penetrations, tests from Almusallam (1995)

6.4 Bond behaviour of corroded reinforcement according to Auyeung (2000)

6.4.1 Description of the performed tests

Auyeng tested concrete prisms in which two steel bars were embedded, see Figure 6.7. Corrosion was accelerated by induced current. The magnitude of the corrosion was measured by the weight loss method. The two reinforcement bars were pulled in the opposite direction. The configuration simulated reinforcement bars in the tension zone. The bond-slip response was reported. In addition, the slip at failure for different corrosion penetration was summarized in a table, see Table 6.4. The post failure response was not reported.

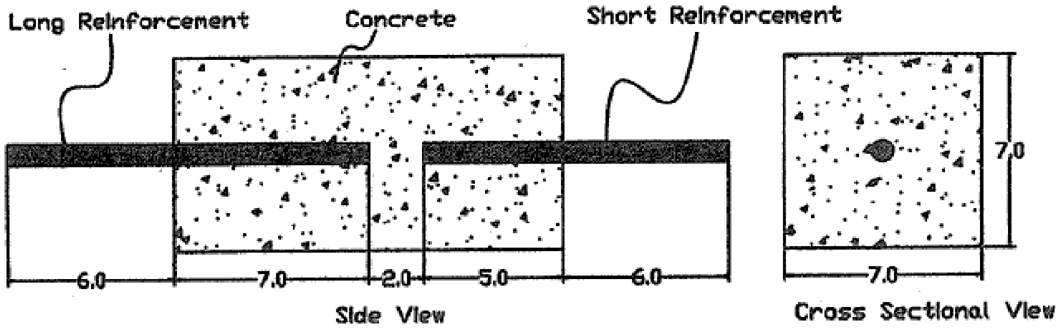

Figure 6.9 Details of specimen, according to Auyeung (2000); (Note: All dimensions are in inch)

6.4.2 Comparison to the method with modified slip

The modified Model Code is not valid for a cover-to-bar diameter ratio of $c_{main} / d =$ 4,2 that has been used in the tests. When looking at the slip at failure it can be seen that it is much higher for uncorroded reinforcement than for corroded reinforcement. This can indicate a change in failure mode that is not considered in the modified Model Code.

By using the reported results, it was possible to study the effect of corrosion on slip at failure. This can be used to verify that the effect of corrosion on radial deformations can be related to the effect of slip on radial deformations.

Due to the assumed change in failure mode the mean slip for a corrosion penetration of $x = 0.036$ mm was compared with the slip at failure for other corrosion penetrations according to equation (6.2). This made it possible to calculate the factor *f*, according to equation (6.3) which relates the effect of corrosion on failure to the effect of slip to failure.

$$s_{crack,x=0.036} + f \cdot 0.036 = s_{crack,x} + f \cdot x \qquad (6.2)$$

$$\Rightarrow f = \frac{\left(s_{crack,x=0.036} - s_{crack,x}\right)}{\left(x - 0.036\right)} \tag{6.3}$$

where

$s_{crack,x=0,036}$	is the mean slip at failure for a corrosion penetration of $x = 0.036$ mm in mm
$s_{crack,x}$	is the slip at failure for a corrosion penetration x in mm
x	is the corrosion penetration in mm

As the slip at failure of sample no. 5 did not fit to the other results it was left without consideration when the mean value, the standard deviation and the coefficient of variance was calculated. A mean value of $f = 1.367$ was obtained, see Table (6.4). That did not agree with the factor of $f = 8.1$ obtained by analysing the parameter study. Some variation of the *f* can be explained by the fact that the descending branch of the bond stresses could not be considered in Auyeung's tests. Even when a small slope of the descending branch of the bond-slip curve is assumed the factor would still be smaller than four; see Figure 6.7.

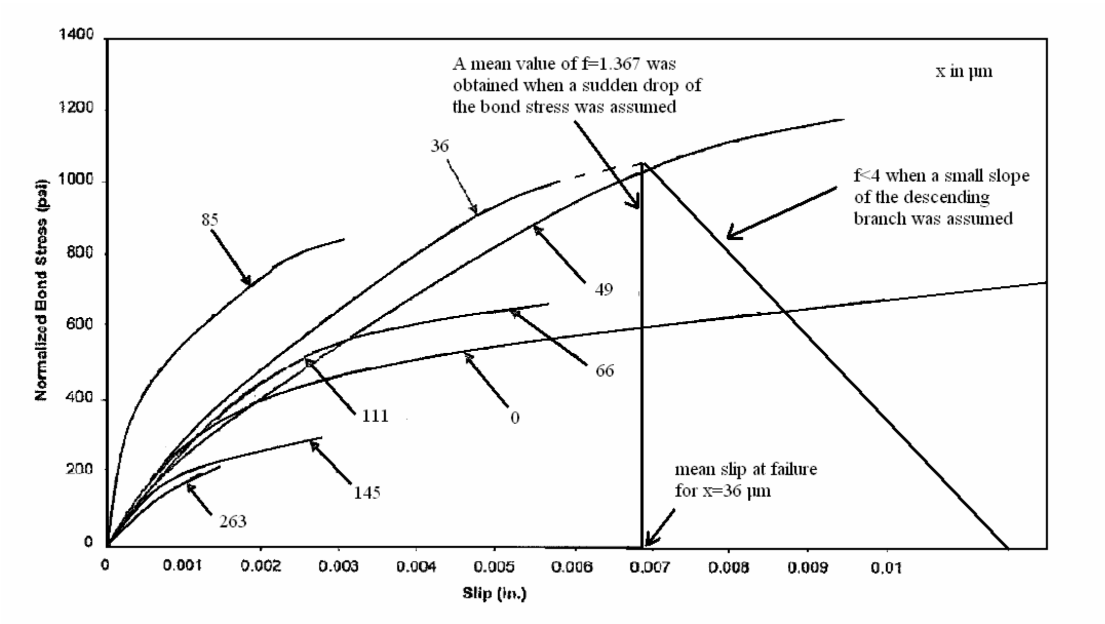

Figure 6.10 Bond-slip curves, modified from Auyeung (2000)

Table 6.4 Slip at failure load for various corrosion penetrations (marked boxes were not considered when the average, standard deviation and the coefficient of variation were calculated), modified from Auyeung (2000)

Sample No.	Corrosion penetration [mm]	slip at failure [mm]	f=($s_{crack,x}$-$s_{crack,x=0.0036}$)/(x-0.0036-x)	$s_{crack,mod}$=$s_{crack,x}$+f•x [mm]
1	0.000	0.660		0.660
2	0.000	0.432		0.432
3	0.036	0.198		0.247
4	0.036	0.147		0.197
5	0.049	0.241	-5.253	0.308
6	0.066	0.142	1.011	0.233
7	0.072	0.091	2.246	0.190
8	0.085	0.079	1.906	0.195
9	0.111	0.066	1.421	0.218
10	0.145	0.061	1.025	0.259
11	0.263	0.038	0.593	0.398
	average:	0.103	1.367	0.242
	standard deviation:	0.051	0.564	0.063
	coefficient of variation:	0.494	0.412	0.262

By using the new obtained factor it was checked whether the failure could be predicted by using the modified slip according to equation (6.4).

$$s_{crack,\mathrm{mod}} = s_{crack,x} + f \cdot x \tag{6.4}$$

A mean value of $s_{crack,\mathrm{mod}} = 0.242\,\mathrm{mm}$ with a coefficient of variation of 26.2% was obtained. For specimens with the same corrosion penetration, the slip at failure was compared without considering the corrosion to get an ideal of the scatter of the tests. A coefficient of variation of 20.9% for specimens one and two and 14.7% for specimens three and four was calculated. As the coefficient of variation of the modified slip at failure was not much higher than for slip at failure for specimens with the same corrosion penetration, it can be assumed that it is possible to relate the effect of corrosion on the effect of slip. Thus, the modified slip seems to be an adequate parameter to take the effect of corrosion into account.

For the sample with the highest corrosion penetration the largest error was obtained when the modified slip at failure was compared with the mean modified slip at failure for the corroded cases. This can indicate that for high corrosion penetrations the factor f is not constant anymore, see Figure 6.11.

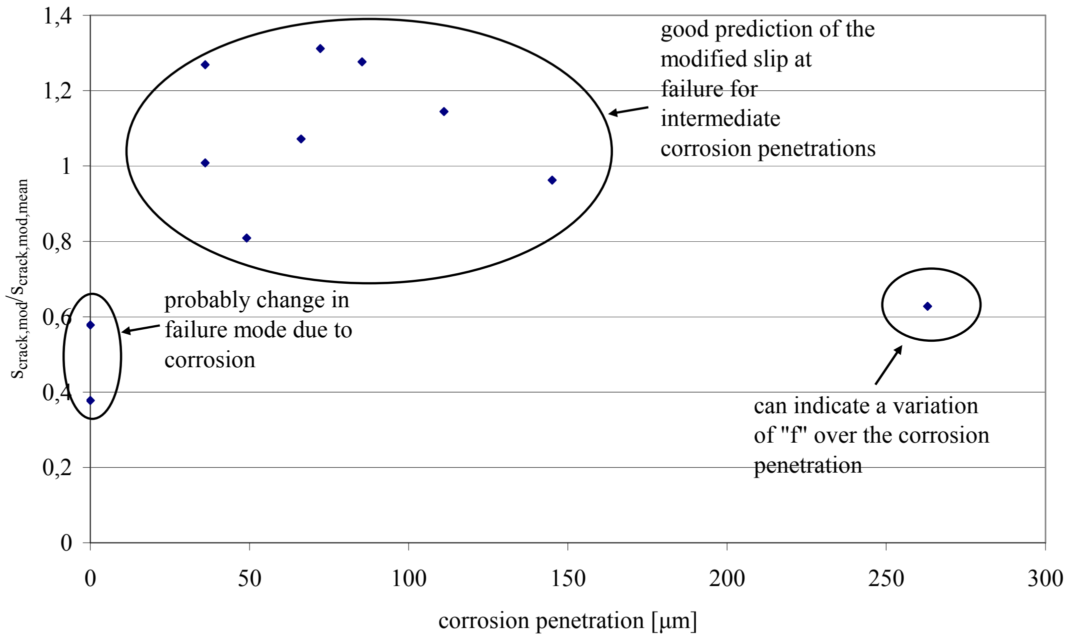

Figure 6.11 Modified slip at failure divided by mean modified slip at failure over the corrosion penetration

6.5 Summary of the verification of the results

When comparing the results from the modified Model Code with tests found in literature the accuracy is not sufficient. Even for uncorroded reinforcement the prediction of the bond strength using the unmodified Model Code is not satisfactory. Hence it is not clear how much error is introduced by the modification of the Model Code. The hypothesis that the effect of corrosion on cracking can be related to the effect of slip on cracking was confirmed by one test series. The factor that was obtained by the parameter study to relate the effect of corrosion to the effect of slip on cracking could not be verified. In addition, a change in failure mode from pull-out to splitting failure due to corrosion could be observed in two tests. As the modified Model Code does not cover this change it can not be applied for geometries that showed pull-out failure for uncorroded reinforcement.

The method described in Chapter 4 showed promising results when it was applied on the parameter study. When it was combined with the bond-slip model of the Model

Code and then compared with performed tests, the results were not satisfactory anymore.

7 Conclusions

7.1 General conclusions

For the analysed parameter study it seems to be possible obtain the bond-slip curve for corroded reinforcement by the bond-slip curve of uncorroded reinforcement. This can be done by shifting the bond-slip curves for uncorroded reinforcement along the slip-axes according to the corrosion penetration of the reinforcement that it now should describe. The shifted bond-slip curve can then be used as an upper limit of the bond stresses for the corroded case. When this method was combined with the bond-model given in the Model Code and then compared to reported test the results were not sufficient anymore.

In addition it seems to be possible to relate the effect of corrosion on cracking to the effect of slip on cracking for specimens that showed splitting failure already for uncorroded reinforcement.

In the parameter study the effect of transverse reinforcement on bond-behaviour of the corroded reinforcement was almost negligible for most studied geometries. This disagrees with reported tests; see Rodriguez (1994) and Fang (2006). That is due to the fact that in the mentioned tests the transverse reinforcement has been provided as stirrups while in the parameter study the transverse reinforcement was modelled as a single bar. If the transverse reinforcement is not provided as stirrups it is not working when the cracks develop parallel to the surface. As the type of the transverse reinforcement occurred to be decisive for the effect on bond, results from tests using stirrups can not be applied to other types of transverse reinforcement.

The development of the bond strength and the dissipated energy is governed by the crack pattern. Only when the cracks pass the transverse reinforcement, it keeps a certain degree of confinement. The most important factor controlling the crack pattern is the concrete cover to bar spacing ratio.

The first cover crack turned out to limit the bond strength when splitting failure is obtained. The most important factor controlling the appearance of the cover crack is the concrete cover to bar diameter ratio.

7.2 Suggestions for further research

The method to obtain bond-slip curves described in Model Code 1990 is not very user-friendly. The linear interpolation between the confined and the unconfined case considering three different parameters is not very applicable. Without a practical model describing the bond-slip response of uncorroded reinforcement it is not possible to develop a convenient model that covers even the corroded cases.

The hypothesis behind the modification of the Model Code 1990 due to reinforcement corrosion has to be validated. Therefore some tests are needed that are within the scope of the method. The mentioned assumptions have to be checked and their application area has to be restricted under the consideration of the expected error.

More information of the factor that relates the splitting expansion of the corrosion products to the radial deformation caused by slip of ribbed bars is needed. Therefore more tests are needed with different geometries and different rib profiles of the reinforcement steel.

The analysed parameter study has shown that transverse reinforcement does not necessarily provide confinement. As this does not agree with performed tests using stirrups as transverse reinforcement, more research is needed to evaluate the effect of leg spacing of the transverse reinforcement on confinement.

8 References

Almusallam A., Al-Gahtani A. S., Aziz A. R. and Rasheeduzzafar (1995): Effect of reinforcement corrosion on bond strength. Construction and Building Materials, Vol. 10, No 2, pp. 123-129

Al-Sulaimani G. J., Kaleemullah M., Basunbul I. A. and Rasheeduzzafar (1990): Influence of corrosion and cracking on bond behaviour and strength of reinforced concrete members. *ACI Structural Journal*, Vol. 87, No. 2, pp. 220-231

Andrade C., Alonso C. and Molina F. (1993): Cover cracking as a function of bar corrosion.1. Experimental test. *Materials and Structures,* Vol 26, No. 162, pp. 453-464

Auyeung Y., Balaguru P. and Chung L. (2000): Bond behaviour of corroded reinforcement bars, *ACI Materials Journal*, Vol. 97, No. 2, pp. 214-220

Balázs G. and Koch R. (1995): Bond Characteristics Under Reversed Cyclic Loading. *Otto Graf Journal,* Vol. 6 1995, pp. 47-62.

Cabrera J. G. and Ghoddoussi P. (1992): The effect of reinforcement corrosion on the strength of the steel/concrete 'bond'. *Bond in Concrete, Proceedings of an International Conference, Riga*, 1992. Comité Euro-International du Béton, pp. 10-11 - 10-24

CEB (1993): *CEB-FIP Model Code 1990*. CEB Bulletin d'Information No. 213/214, Lausanne 1993.

CEB (2000): *CEB-FIB Bond of reinforcement in concrete.* CEB Bulletin d'Information No. 10, Lausanne 2000, pp.188-215.

Esfahani M. R., Rangan B.V. (2000): Influence of transverse reinforcement on bond strength of tensile splices. *Cement & Concrete Composites* No. 22, 2000, pp.159-163

Fang C., Lundgren K., Liuguo C. and Chaoying Z. (2004): Corrosion influence on bond in reinforced concrete. *Cement and Concrete Research* No. 34 (2004) pp. 2159-2167

Ghandehari M., Zulli M. and Shah S. P. (2000): Influence of corrosion on bond degradation in reinforced concrete. *Proceedings EM2000, Fourteenth Engineering Mechanics Conference,* Austin, Texas, 2000. American Society of Civil Engineering, Reston, VA, pp.1-15

Liu Y. P. and Weyers R. E. (1998): Modelling the time to corrosion cracking in chloride contaminated reinforced concrete structures. *ACI Materials Journal*, Vol. 95, No. 6, pp. 675-681

Lundgren K. (1999): *Modelling of Bond: Theoretical Model and Analyses.* Division of Concrete Structures, Chalmers University of Technology, Report 99:5, Göteborg, Sweden, 1999

Lundgren K. (2005a): Bond between ribbed bars and concrete. Part 1: Modified model. *Magazine of Concrete Research*, Vol. 57, No. 7, September, pp. 371-382

Lundgren K. (2005b): Bond between ribbed bars and concrete. Part 2: The effect of corrosion. *Magazine of Concrete Research*, Vol. 57, No. 7, September, pp. 383-395

Magnusson J (1997): *Bond and Anchorage of Deformed Bars in High-Strength Concrete*. Licentiate Thesis. Division of Concrete Structures, Chalmers University of Technology, Publication 97:1, Göteborg 1997.

Rasheeduzzafar, Al-Saadoun S. S. and Al-Gahtani A. S. (1992): Corrosion cracking in relation to bar diameter, cover and concrete quality. *Journal of Materials in Civil Engineering*, Vol. 4, No. 4. pp. 327-342

Rodriguez J., Ortega L., Garcia A. (1994): Corrosion of reinforcing bars and service life of reinforced concrete structures: Corrosion and bond deterioration. Int. Conference, *Concrete across borders,* Denmark, Vol, II, pp. 315-326

San-Roman A. (2006): *Bond behaviour of corroded reinforcement.* Master Thesis 2006:94. Department of Structural Engineering, Chalmers University of Technology, Göteborg, Sweden, 2006

Shima H. (2002): Local bond stress-slip relationship of corroded steel bars embedded in concrete. *Proceedings of the 3rd International Symposium: Bond in Concrete-from research to standards-*, Budapest, Hungary. Internatinal Federation for Structural Concrete and Hungarian Group of FIP, pp. 153-158

Tepfers R. (1973): *A Theory of Bond Applied to Overlapped Tensile Reinforcement Splices for Deformed Bars.* Ph.D. Thesis. Division of Concrete Structures, Chalmers University of Technology, Publication 73:2, Göteborg, Sweden, 1973

APPENDIX A Summary of the parameter study

In the first column the name of each specimen is given. The factor differing from the mean analysis is usually chosen as the name, i.e. "C20" denotes a specimen with a concrete type "C20" instead of "C40" for the mean geometry. Under the name of each specimen the ratio between the concrete cover of the main reinforcement to the top surface and the clear bar spacing to the side, c_{main}/w_{clear}, is calculated.

In the second column the different corrosion penetrations, x, are reported. In column 3 to 6 the parameter defining the geometry are shown. The concrete strength is reported in the 7th column.

In column 8 the bond strength is shown. To study the development of the bond strength over the corrosion penetration the bond-strength for corroded cases was divided by the bond strength for the uncorroded case. The quotient is called normalized bond strength shown in column 9.

In column 10 the area under the bond-slip curve, F, is calculated. The area represents the dissipated energy. As some analyses did not converge the calculated area was limited to the slip, s_{conv}, till which most analyses showed convergence. This slip is reported in column 10, too. For analyses that showed severe problems to get convergence, even for earlier stages the dissipated energy is not calculated and the cell is marked. As s_{conv} differed for the different specimens the comparison of the area under the bond-slip curves between theses specimens can lead to wrong conclusions. Therefore the next column shows the normalized dissipated energy to see the development depending on the corrosion penetration. To normalize the dissipated energy it was divided by the dissipated energy of the uncorroded case.

To get more information about the bond stiffness development the slip that caused the maximum bond stresses is shown in column 12. In the next column the slope of a line from the origin of the bond-slip curve to the maximum bond stress with its related slip was calculated, see Figure 3.5. This slope, φ, representing a kind of secant stiffness, was again normalized by the uncorroded case in the next column.

The next column indicates the obtained crack patterns that are described in detail in Chapter 3.4-3.7. In column 15 the slip that led to the first cover crack is reported. For cases that already cracked for the applied corrosion, the critical corrosion penetration is reported and the cell is marked. The next column contains the same information as column 15 but now for the development of the second cover crack.

In column 17 a factor, f, is calculated that relates the effect off corrosion to the effect of slip. For more information about that factor see Chapter 3.2.3.

In column 18 the factor, f, is used to calculate the effective slip at failure according to equation (4.6).

1 Name	2 corrosion penetration x[μm]	3 half width w/2 [mm]	4 main concrete cover c_{main}[mm]	5 main bar diameter d_{main}[mm]	6 amount of transverse reinforcement d_t[cm^2/m]	7 concrete strength f_{ck}[MPa]	8 Bond strength τ_{max}[Mpa]	9 normalized Bond strength $\tau_{max,n}$	10 Dissipated energy F [Nmm/mm^2]	11 normalized Area under the bond-slip curve F_n	12 slip for maximum bond stress $s(\tau_{max})$[mm]	13 secant stiffness for maximum bond stress φ[N/m^3]	14 cracking mode number	15 loading 1[st] cover crack s[mm];x[μm]	16 loading 2[nd] cover crack s[mm];x[μm]	17 Factor; f	18 s_{eff} at failure [mm]
									s_{conv}=1.3 mm								
Mean	0	50	30	20	2.62	40	11.34	1.00	8.73	1.00	0.28	41.3	3	0.27	1.35		0.27
Nr. 1	10	50	30	20	2.62	40	11.23	0.99	8.27	0.95	0.20	56.2	3	0.2	1.2	7.0	0.28
	25	50	30	20	2.62	40	10.30	0.91	7.39	0.85	0.08	137.4	3	0.08	0.95	7.8	0.28
c_{main}/w_{clear}	50	50	30	20	2.62	40	7.09	0.62	7.00	0.80	0.05	141.8	3	30	0.9	9.0	0.24
0.375	100	50	30	20	2.62	40	5.99	0.53	6.12	0.70			3	30	0.33		0.24
	200	50	30	20	2.62	40	5.90	0.52					3	30			0.24
									s_{conv}=0.78 mm								
C20	0	50	30	20	2.62	20	7.43	1.00	4.16	1.00	0.22	34.5	2	0.19	0.83		0.19
Nr. 2	10	50	30	20	2.62	20	7.20	0.97	4.10	0.99	0.13	57.6	2	0.18	0.8	1.5	0.26
	25	50	30	20	2.62	20	5.59	0.75	3.54	0.85	0.10	55.9	2	20	0.73	9.5	0.16
c_{main}/w_{clear}	50	50	30	20	2.62	20	4.82	0.65	2.26	0.54	0.08	64.2	2	20	0.35		0.16
0.375	100	50	30	20	2.62	20	1.37	0.18	0.73	0.17	0.15	9.1	2	20	56		0.16
	200	50	30	20	2.62	20	0.00	0.00					2				
									s_{conv}=1.8 mm								
C80	0	50	30	20	2.62	80	17.28	1.00	15.20	1.00	0.33	53.2	3	0.38			0.38
Nr. 3	10	50	30	20	2.62	80	17.11	0.99	14.47	0.95	0.28	62.2	3	0.3		7.5	0.38
	25	50	30	20	2.62	80	16.26	0.94	13.88	0.91	0.18	92.9	3	0.23		6.0	0.43
c_{main}/w_{clear}	50	50	30	20	2.62	80	1.84	0.11	2.06	0.14	0.03	73.6	1	40		9.4	0.33
0.375	100	50	30	20	2.62	80	1.20	0.07	1.98	0.13			1	40			0.33
	200	50	30	20	2.62	80	1.21	0.07	0.64	0.04			1	40			0.33
									s_{conv}=1.3 mm								
dt=10-150	0	50	30	20	5.24	40	11.42	1.00	4.54	1.00	0.28	41.5	3	0.27	0.48		0.27
Nr. 4	10	50	30	20	5.24	40	11.28	0.99	4.11	0.91	0.20	56.4	3	0.2	0.38	6.5	0.28
	25	50	30	20	5.24	40	10.31	0.90	2.14	0.47	0.10	103.1	3	0.1	0.15	6.6	0.30
c_{main}/w_{clear}	50	50	30	20	5.24	40	8.00	0.70	0.95	0.21	0.05	160.0	3	32	0.03	8.3	0.26
0.375	100	50	30	20	5.24	40	0.90	0.08	1.00	0.22			3	32			0.26
	200	50	30	20	5.24	40	1.17	0.10	0.87	0.19			3	32			0.26

									s_{conv}=1.4 mm							
no transverse	0	50	30	20	0.00	40	10.87	1.00	3.54	1.00	0.26	42.6	2	0.26	1.2		0.26
reinforcement	10	50	30	20	0.00	40	10.68	0.98	3.54	1.00	0.18	61.0	2	0.2	1.15	6.0	0.28
Nr. 5	25	50	30	20	0.00	40	6.01	0.55	2.38	0.67	0.05	120.3	2	25	1.1	10.4	0.20
c_{main}/w_{clear}	50	50	30	20	0.00	40	2.47	0.23	1.39	0.39	0.05	49.4	2	25	1.1		0.20
0.375	100	50	30	20	0.00	40	1.23	0.11	0.50	0.14	0.05	24.6	2	25	1.15		0.20
	200	50	30	20	0.00	40	0.15	0.01	0.16	0.05	0.02	10.0	2	25	1.1		0.20
									s_{conv}=0.8 mm							
d=25	0	50	30	25	2.62	40	11.80	1.00	6.02	1.00	0.25	47.2	4	0.25	0.75		0.25
Nr. 6	10	50	30	25	2.62	40	11.74	0.99	5.41	0.90	0.18	67.1	4	0.18	0.63	7.5	0.26
	25	50	30	25	2.62	40	10.49	0.89	4.03	0.67	0.06	174.9	4	0.08	0.48	7.0	0.28
c_{main}/w_{clear}	50	50	30	25	2.62	40	8.67	0.73	2.66	0.44	0.08	115.6	4	27	0.3	9.3	0.22
0.400	100	50	30	25	2.62	40	1.74	0.15	0.90	0.15	1.50	1.2	4	27	78		0.22
	200	50	30	25	2.62	40	1.17	0.10	0.28	0.05	0.05	23.3	4	27	78		0.22
									s_{conv}=1.2 mm							
d=10	0	50	30	10	2.62	40	9.34	1.00	5.56	1.00	0.35	26.7	3	0.35	0.98		0.35
Nr. 7	10	50	30	10	2.62	40	9.04	0.97	5.07	0.91	0.28	32.9	3	0.3	0.95	5.0	0.38
	25	50	30	10	2.62	40	8.24	0.88	4.41	0.79	0.15	55.0	3	0.23	0.75	5.0	0.43
c_{main}/w_{clear}	50	50	30	10	2.62	40	5.25	0.56	3.92	0.70	0.08	69.9	3	43	0.75	8.1	0.35
0.333	100	50	30	10	2.62	40	3.63	0.39	2.93	0.53	0.10	36.3	3	43	0.35		0.35
	200	50	30	10	2.62	40	0.71	0.08	0.57	0.10			3	43			0.35
									s_{conv}=1.0mm							
w/2=150	0	150	30	20	2.62	40	11.34	1.00	7.31	1.00	0.28	41.3	3	0.3			0.30
Nr. 8	10	150	30	20	2.62	40	11.23	0.99	7.02	0.96	0.18	64.2	3	0.23		7.5	0.31
	25	150	30	20	2.62	40	10.30	0.91	6.68	0.91	0.08	137.4	3	0.13		7.0	0.33
c_{main}/w_{clear}	50	150	30	20	2.62	40	7.09	0.62	5.83	0.80	0.05	141.8	3	30		10.0	0.24
0.107	100	150	30	20	2.62	40	5.99	0.53	4.76	0.65	0.10	59.9	3	30			0.24
	200	150	30	20	2.62	40	5.91	0.52	3.75	0.51			3				
									s_{conv}=0.8 mm							
w/2=75	0	75	30	20	2.62	40	11.17	1.00	5.47	1.00	0.27	42.2	3	0.3			0.30
Nr. 9	10	75	30	20	2.62	40	10.83	0.97	5.83	1.06	0.18	61.9	3	0.23		7.5	0.31
	25	75	30	20	2.62	40	10.07	0.90	5.27	0.96	0.08	134.3	3	0.13		7.0	0.33
c_{main}/w_{clear}	50	75	30	20	2.62	40	7.28	0.65	4.50	0.82	0.05	145.5	3	28	1.15	10.7	0.23
0.231	100	75	30	20	2.62	40	5.08	0.45	3.98	0.73	0.05	101.7	3	28	0.83		0.23
	200	75	30	20	2.62	40	3.82	0.34	2.84	0.52			3				
									s_{conv}=0.6 mm							
c=45	0	50	45	20	2.62	40	13.33	1.00	2.94	1.00	0.33	41.0	1	0.35			0.35
Nr. 10	10	50	45	20	2.62	40	13.07	0.98	2.79	0.95	0.25	52.3	1	0.28		7.5	0.36
	25	50	45	20	2.62	40	12.14	0.91	1.69	0.58	0.13	97.1	1	0.15		8.0	0.35
c_{main}/w_{clear}	50	50	45	20	2.62	40	0.85	0.06	0.39	0.13	0.02	42.4	1	32		10.9	0.26

0.563	100	50	45	20	2.62	40	0.64	0.05	0.35	0.12	0.63	1.0	1	32			0.26
	200	50	45	20	2.62	40	0.45	0.03	0.23	0.08			1	32			0.26
									s_{conv}=0.4 mm								
c=45	0	50	45	20	2.62	40	13.33	1.00	2.74	1.00	0.33	41.0	1	0.35			0.35
d=10-150	10	50	45	20	2.62	40	13.07	0.98	2.51	0.91	0.25	52.3	1	0.28		7.5	0.36
Nr. 11	25	50	45	20	2.62	40	11.55	0.87	1.20	0.44	0.10	115.5	1	0.13		9.0	0.33
c_{main}/w_{clear}	50	50	45	20	2.62	40	1.03	0.08	0.33	0.12	0.03	41.0	1	30		11.7	0.24
0.563	100	50	45	20	2.62	40	0.70	0.05	0.27	0.10			1	30			0.24
	200	50	45	20	2.62	40	0.81	0.06	0.25	0.09			1	30			0.24
									s_{conv}=0.4 mm								
c=45; no transverse	0	50	45	20	2.62	40	13.79	1.00	3.09	1.00	0.35	39.4	1	0.38			0.38
reinforce ment	10	50	45	20	2.62	40	13.51	0.98	3.02	0.98	0.28	49.1	1	0.3		7.5	0.38
Nr. 12	25	50	45	20	2.62	40	12.09	0.88	1.91	0.62	0.13	96.7	1	0.13		10.0	0.33
c_{main}/w_{clear}	50	50	45	20	2.62	40	3.72	0.27	1.08	0.35			1	34		11.0	0.28
0.563	100	50	45	20	2.62	40	3.87	0.28	1.16	0.38			1	34			0.28
	200	50	45	20	2.62	40	3.56	0.26	1.22	0.40			1	34			0.28
									s_{conv}=0.8 mm								
Mean	0	50	30	20	2.62	40	11.12	1.00	5.19	1.00	0.27	41.2	2	0.3	0.78		0.30
other mesh	10	50	30	20	2.62	40	10.68	0.96	5.27	1.02	0.18	61.0	2	0.23	0.73	7.5	0.31
Nr. 13	25	50	30	20	2.62	40	9.70	0.87	4.00	0.77	0.08	129.3	2	0.13	0.5	7.0	0.33
c_{main}/w_{clear}	50	50	30	20	2.62	40	6.59	0.59	3.68	0.71	0.08	87.9	2	30	0.38	10.0	0.24
0.375	100	50	30	20	2.62	40	2.94	0.26	2.08	0.40	0.10	29.4	2	30	86		0.24
	200	50	30	20	2.62	40	3.03	0.27	2.33	0.45	0.40	7.6	2	30	86		0.24
													Average:			8.1	0.3
													Standard deviation:			1.70	0.06
													Coefficient of variance			0.21	0.21